2015

Biophysical Characterization Of The Folding, Membrane Topology And Ion Transport Activity Of Ucp2 Using Selective Trp Mutants

Tyler C. Auld
Wilfrid Laurier University, auld0440@mylaurier.ca

BIOPHYSICAL CHARACTERIZATION of the FOLDING, MEMBRANE TOPOLOGY and ION TRANSPORT ACTIVITY of UCP2 using SELECTIVE Trp MUTANTS

By

Tyler Auld

B.Sc. Biochemistry and Biotechnology, Wilfrid Laurier, 2013

THESIS

Submitted to the Department of Chemistry and Biochemistry

In partial fulfilment of the requirements for

Master of Science in Chemistry

Wilfrid Laurier University

ABSTRACT

Human Uncoupling Protein 2 (hUCP2) is one of five known human UCPs which are found in the inner mitochondrial membrane and have been shown to facilitate the translocation of protons from the intermembrane space to the mitochondrial matrix. The detailed physiological role of UCP2 proton transport, the mechanism by which it mediates this proton transport, as well as its structure has also yet to be elucidated. In order to help determine the topology of UCP2 embedded in the membrane as well as its mechanism of proton transport, the intrinsic fluorescence properties of the two tryptophan residues (Trp) present in its structure (W176 and W283) were used. To this end, three substitution mutants were created by site-directed mutagenesis using primer overlap-extension PCR; these were: W176Y, W283F and W176Y-W283F. The three mutant cDNAs then introduced into a membrane-targeted bacterial expression system from which they were then expressed in *E. coli* and purified via autoinduction and immobilized metal affinity chromatography (IMAC). Fluorescence and circular dichroism spectroscopy were then used to confirm that the mutants retained native-like conformations. Fluorescence quenching assays with acrylamide were performed to probe the topology of UCP2 embedded in the membrane via the differing accessibility of each Trp to the acrylamide quencher. The final stage of this project involved probing the effects of the Trp residues on the proton transport activity of UCP2 via a proton transport assay previously developed in our lab. Unfortunately, the presence of high background fluorescence, as seen in the W176Y-W283F fluorescence spectra with excitation at 295nm, either due to tryptophan containing-proteinaceous contaminants in the sample, or the presence of a deprotonated tyrosine residue (tyrosinate) in the folded structure of UCP2, has made it impossible to draw any definitive conclusions from the intrinsic fluorescence assays. The results of the proton transport assay for the W176Y-W283F Trp mutant and wt UCP2 indicate a role for the conserved UCP Trp residues in the proton transport activity of the protein based on a 26.7% reduction in the transport rate of the double mutant in comparison to the wt protein.

ACKNOWLEDGEMENTS

I would like to acknowledge my supervisor, Dr. Masoud Jelokhani-Niaraki for his support and encouragement throughout the past four years in the lab and for believing in me enough to give me this opportunity at a time when I needed encouragement most. Under his guidance I feel I have grown immensely not only as a student but as a person as well. I would also like to thank Dr. Matthew Smith for allowing me access to his laboratory and equipment for completing the molecular biology aspects of this project and also for technical assistance and encouragement throughout the project. Next, I need to thank Dr. Patrick (Tuan) Hoang, whose help developing the project was invaluable and whose support helped keep me moving forward through the more difficult aspects of this project. I have trouble imagining a better colleague and I am proud to call him a friend. I would also like to thank the remaining members of my committee, Dr. Allison McDonald and Dr. Lillian DeBruin for their knowledge, time, patience and consideration throughout the past two years, especially with respect to troubleshooting and the delays encountered. I would like to thank Tu Hoang, our lab technician for her assistance in the lab throughout the project. I would like to thank all of the colleagues I have had the opportunity to work with in the Jelokhani and Smith labs throughout the past two years of graduate studies as well as the last two years of my undergraduate degree including: James Campbell, Stephanie Uwumarenogie, Howard Teresinski, Mark Ecclestone, Tijana Matovic, Brittany Porter and Nick Grimberg among, others. Finally, I would like to thank my family for their constant support and encouragement throughout my education.

DECLARATION OF WORK PERFORMED

All data presented and described in this thesis are the results of my own work.

LIST OF TABLES

LIST OF FIGURES

LIST OF ABBREVIATIONS

ADP	**Adenosine Diphosphate**
ANT	**Adenine Nucleotide Translocator**
ATP	**Adenosine Triphosphate**
BAT	**Brown Adipose Tissue**
BLAST	**Basic Local Alignment Search Tool**
BSA	**Bovine Serum Albumin**
CD	**Circular Dichroism**
ETC	**Electron Transport Chain**
FFA	**Free Fatty Acid**
GDP	**Guanosine Diphosphate**
GTP	**Guanosine Triphosphate**
IMAC	**Immobilized Metal Affinity Chromatography**
LDAO	**Lauryldimethylamine-oxide**
NMR	**Nuclear Magnetic Resonance**
NTA	**Nitrilotriacetic Acid**
OG	**Octyl Glucoside**
PCR	**Polymerase Chain Reaction**
ROS	**Reactive Oxygen Species**
SDS	**Sodium Dodecyl Sulfate**
THP	**Tris(hydroxypropyl)phosphine**
UCP	**Uncoupling Protein**

1 UNCOUPLING PROTEIN 2

1.1 Cellular Energy Production in Mitochondria: Proton Motive Force, ATP Synthesis and Uncoupling

In eukaryotic cells, mitochondria are analogous to a power plant in that they convert energy into a usable form which may then be used to do work. In the case of the mitochondria this energy is obtained from the oxidation of molecules derived from food, and converted to adenosine triphosphate (ATP) through a process known as oxidative phosphorylation and the work done includes, among many things, most anabolic cellular processes. These organelles are enclosed by an outer membrane, which serves mainly as a protective barrier, and also contain an inner membrane, which has tightly controlled permeability. The inner mitochondrial membrane also has a high protein content and is a crucial component for the function of the organelle. As mentioned above, the harnessing of chemical energy as ATP by mitochondria occurs mainly via oxidative phosphorylation, a process which involves the addition of a phosphate group to ADP to form ATP and is catalyzed the enzyme F_1/F_0 ATP synthase. The oxidative phosphorylation catalysed by F_1/F_0 ATP synthase is driven by the controlled dissipation of a proton gradient, which is generated across the mitochondrial inner membrane by the proton pumping activity of complexes I, III and IV of the electron transport chain (ETC). More specifically, oxidation of nutrient molecules obtained from food intake leads to the reduction of

the electron carriers NAD^+ and FAD to NADH and $FADH_2$, respectively. The reduced electron carriers, NADH and $FADH_2$, then pass their electrons on to complexes I and II, respectively, of the ETC which are then passed down the ETC to complex IV where the electrons are then involved in the synthesis of water and via the catalytic reduction of molecular oxygen. As was mentioned, this electron transfer down the ETC leads to the translocation of protons from the mitochondrial matrix to the intermembrane space via the proton pumping activity of complexes I, III and IV, that in turn leads to the generation of both an electrical and chemical potential across the membrane, which together are commonly referred to as the proton motive force. It is this proton motive force that then drives the catalytic activity of F_1/F_0 ATP synthase, which occurs via the passage of protons back through the F_0 domain which in turn drives the rotation and resulting conformational change in the F_1 domain that causes the addition of inorganic phosphate (P_i) to ADP to form ATP (figure 1) [1].

It has been observed, that the proton motive force that is generated as a result of substrate oxidation in the mitochondria is not completely coupled to oxidative phosphorylation by F_1/F_0 ATP synthase and it has been found that coupling efficiency is as low as 50-65% in isolated rat skeletal muscle and 25-30% in cultured human β-cells and up to 25% of the basal metabolic rate of rates may be due to the futile cycling of protons between the intermembrane space and the matrix[2-5]. Moreover, it has also been observed that the coupling efficiency decreases exponentially as the proton motive force increases [5]. This proton leak, which uncouples the oxidation of food derived substrates from oxidative

phosphorlyation has been shown to be mediated through the activity of various members of the mitochondrial anion carrier family of proteins, which are expressed in the inner mitochondrial membrane and which, as their name suggests, facilitate the transport of various anions across this membrane. Some examples of such proteins include: the adenine nucleotide translocase (ANT), mitochondrial phosphate carrier protein (SLC25A3), glutamate aspartate transporter (GLAST or SLC1A3), and uncoupling proteins (UCPs) [5,6,7]. As of yet, the physiological role of this anion carrier protein mediated uncoupling is not well established, with the exception being the case of uncoupling protein 1 (UCP1), whose uncoupling activity plays a well-established role in the process of non-shivering thermogenesis in the brown adipose tissue (BAT) of mammals [5]. Other less conclusively confirmed roles for the uncoupling of the mitochondrial proton from ATP synthesis via oxidative phosphorylation that have been proposed are the attenuation of mitochondrial reactive oxygen species (ROS) production, protection from obesity, regulation of fatty acid metabolism, regulation of insulin secretion by pancreatic β-cells, nutrient sensing and metabolic regulation in the brain as well as adaptive thermoregulation [8].

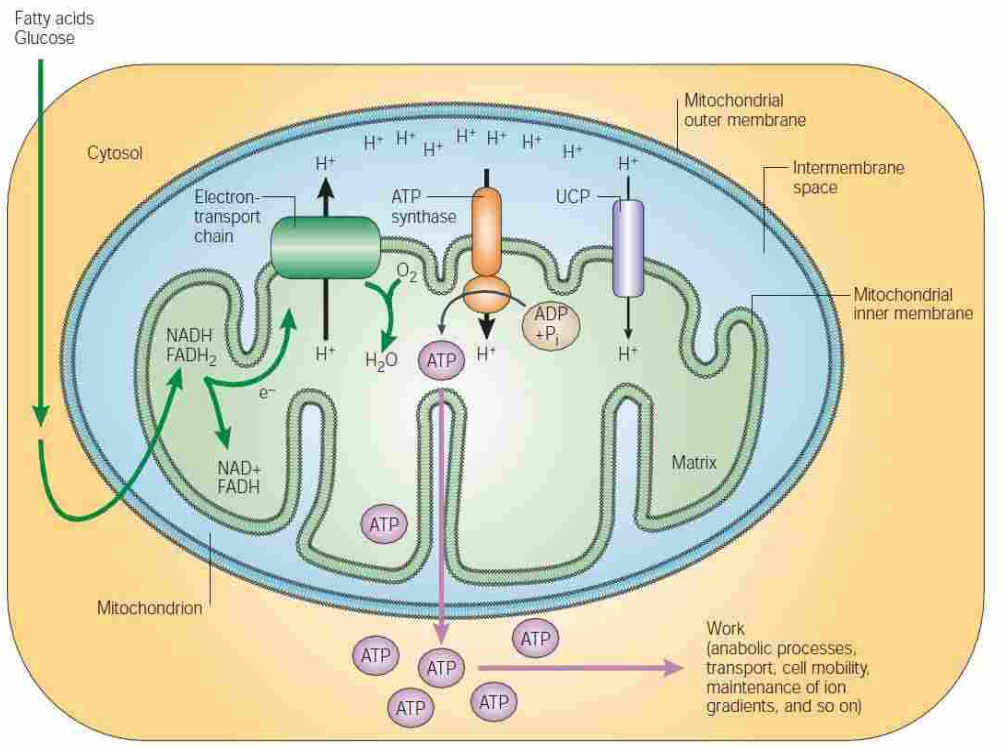

Figure 1: General Representation of Energy Harnessing by Mitochondria: A diagram depicting a general view of energy production in the mitochondria and how UCPs uncouples substrate oxidation from energy production. In general: the oxidation of substrate molecules obtained from food leads to the reduction of electron carriers, which in turn reduce complexes within the electron transport chain. These complexes then pass the electrons on through a total of 4 complexes, which leads to the production of an electrochemical gradient by the pumping of protons across the intermembrane space by complexes I, III and IV. The electrochemical gradient is then used to drive ATP synthesis by F_1/F_0 ATP synthase or alternatively, the electrochemical gradient can be dissipated by UCPs in a manner that does not produce ATP [23].

1.2 The Mitochondrial Uncoupling Proteins

In humans and most other mammals there are 5 known UCP homologues that are expressed, named UCP1-5, in order of discovery. UCP1, by virtue of its exceptionally high expression levels in BAT and consequently its discovery 19 years prior to the discovery of the second UCP, UCP2, (in 1978 and 1997, respectively) is the most extensively characterised UCP and serves as the archetype for investigating the catalytic mechanisms and functions of the other UCP homologues

and these properties will be discussed in detail below [8,9]. Currently there are no high resolution crystal structures available for any of the 5 UCP homologues, although a speculative model based on molecular modelling and comparison with the crystal structure of ANT, which is in the same family of proteins as the UCPs, proposes that the three dimensional structures of the UCPs share a very similar tripartite folding motif with ANT [11,12](see figures 2 and 3). This tripartite folding motif consists of 3 pseudo-repeats, each containing two transmembrane α-helices connected by loop regions, which, along with the amine and carboxy termini, are oriented towards the intermembrane space [11]. This putative model for the structure of the UCPs has been supported by the work of *Berardi et al.* which used the technique of nuclear magnetic resonance (NMR) fragment searching to probe the structure of UCP2 and confirmed that the structure of UCP2 shares the same overall folding motif as ANT (figures 2 and 3) [13].

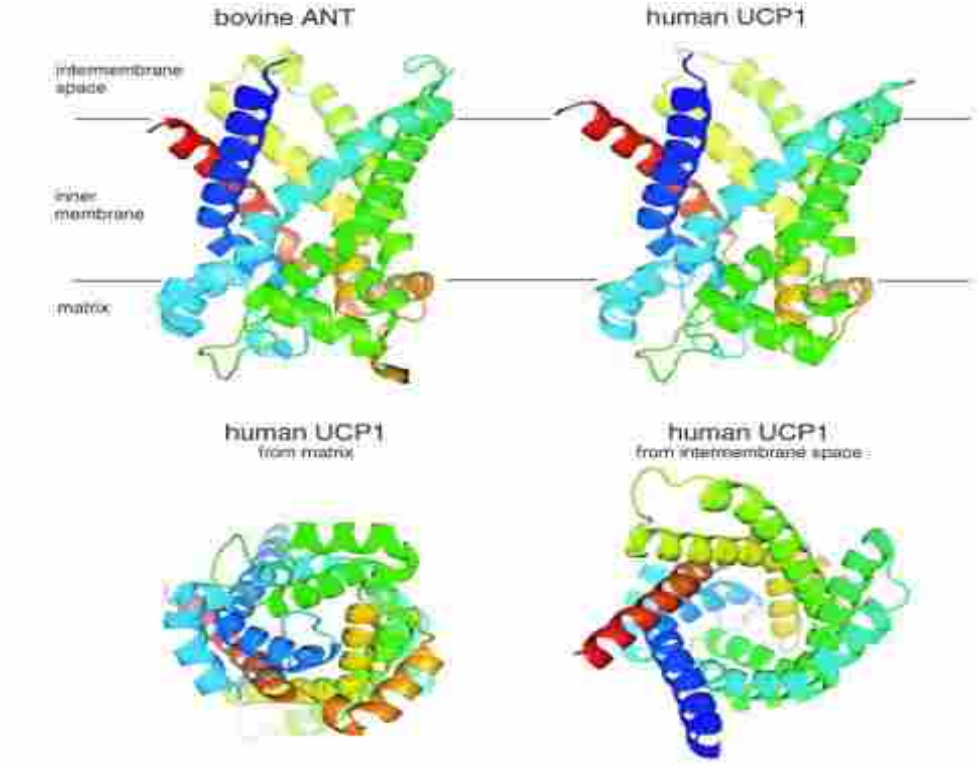

Figure 2: Comparison of Bovine ANT1 to Predicted Structure of UCP2 from Molecular Modelling: The proposed model of human UCP1 based on comparison to the structure of the bovine ANT using the MODELLER molecular modelling program showing side and top views (top and bottom, respectively) [11].

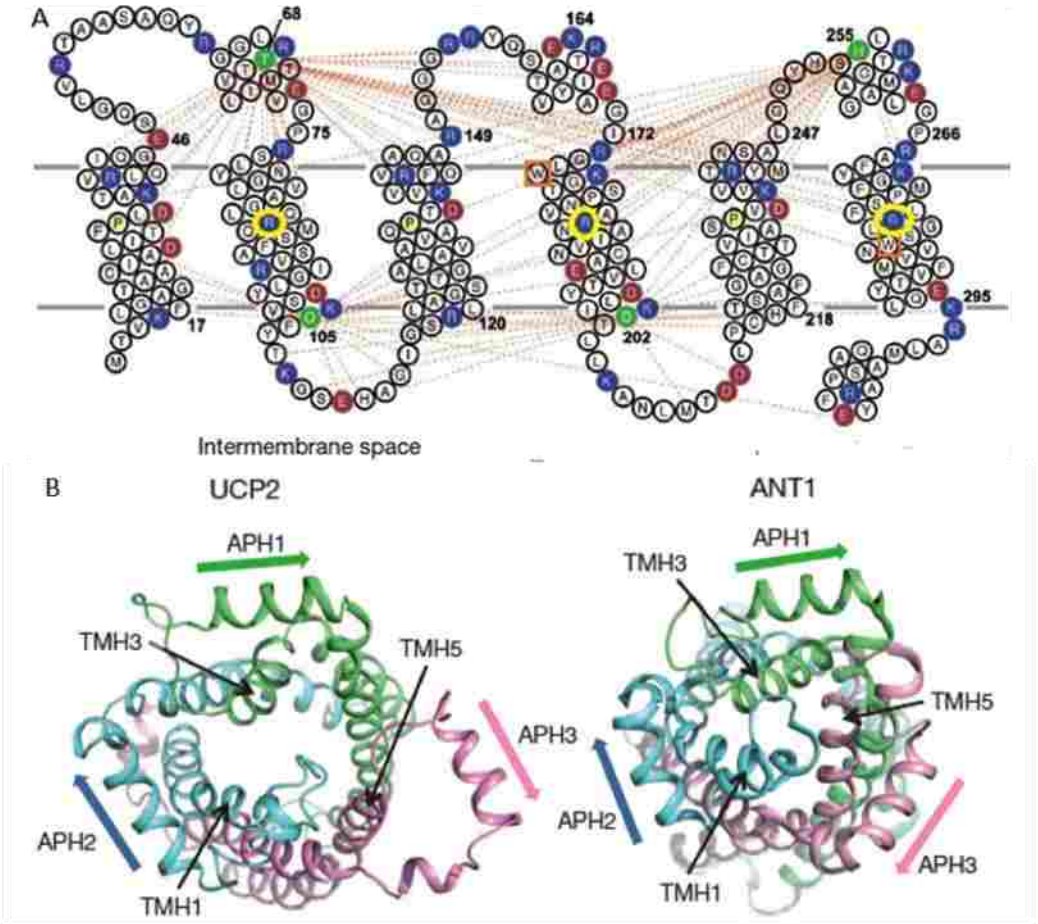

Figure 3: Comparison of Bovine ANT1 to Predicted Structure of UCP2 from NMR Fragment Searching: (A) The membrane topology of the primary sequence of UCP2, based on NMR fragment searching, the two tryptophan residues (W) present in UCP2 are highlighted with orange squares and the three arginine residues involved in nucleotide binding are highlighted with yellow circles [13]. (B) A comparison of the proposed model of UCP2 with ANT1 from the matrix side, showing overall similar structures with the most striking differences occurring in the thirds pseudo repeat (pink) [13].

1.2.1 Uncoupling Protein 1 – The Archetypal Uncoupling Protein

UCP1 is a 33 kDa protein that is expressed at high levels in the mitochondria of the BAT found in mammals, which is primarily involved in the maintenance of body temperature in response to cold through a process known as non-shivering thermogenesis [8,9]. The primary role of UCP1 in mediating this non-shivering thermogenesis occurs through the direct mediation of proton leak in the mitochondria, as well as certain other

aspects of its activity, such as: transport of certain anions, including Cl^-, and fatty acid anions; activation by free fatty acids (FFAs); and inhibition by purine di- and tri-nucleotides (ADP, ATP, GDP and GTP), have been well established [8-11]. The thermogenic activity of UCP1 arises from its ability to catalyse the leak of protons across the inner mitochondrial membrane, from the intermembrane space to the matrix, in a manner that does not drive oxidative phosphorylation and instead releases some of the energy stored in the mitochondrial proton gradient as heat, in response to activation by FFAs, through a β-adrenergic receptor mediated pathway [8]. Despite the fact that UCP1's ability to facilitate proton leak in the mitochondria is so well established, the exact mechanism of this leak, to date, remains elusive for UCP1 and all of its homologues. Due to its well characterised activity, in addition to its clearly demonstrated physiological role in BAT, UCP1 serves as a useful archetype in the study of the rest of the UCP homologues.

1.2.2 Uncoupling Protein Homologues – UCP2-5

The uncoupling protein homologues UCP2-5 have been identified more recently, starting with the discovery of UCP2 in 1997, followed by UCP3 later in 1997, UCP4 in 1999 and UCP5, which was discovered in 1998 as brain mitochondrial carrier protein-1 (BMCP1) but not identified as a member of the uncoupling protein family until after the discovery of UCP4 [9, 14-18]. Since their discovery, it has been confirmed that these UCP homologues share many of the characteristic features of UCP1, such as transport of protons from the intermembrane space, activation by FFAs, and inhibition of the aforementioned proton conductance in the presence of purine di- and tri-nucleotides [8]. However, in contrast with UCP1, while several physiological roles have been proposed for the uncoupling protein homologues, as of yet none of these is definitively established. A common feature of most of the proposed roles for the uncoupling protein homologues is that they involve the protection of the cells they are expressed in from the production and harmful downstream

effects of ROS. This proposed ability of the UCP homologues to attenuate the production would seem logical given the observations that: 1) mitochondria are the main site of ROS production in the cell, with superoxide being produced as a result of the escape of electrons from complexes I and III of the ETC; 2) even slight increases in the mitochondrial membrane potential lead to substantial rises in ROS production 3) UCPs, through their capacity to dissipate the mitochondrial membrane potential, have the potential to ameliorate this increase in ROS production and 4) in the case of UCP2 and UCP3, there is strong experimental evidence for their activation by superoxide radicals, as well as downstream ROS, such as 4-hydroxy-2-nonenal (HNE) and carbon centred lipid radicals [8, 19-22].

1.2.3 The Proposed Mechanisms of Proton Transport by Uncoupling Proteins

The mechanism by which the UCPs mediate their proton and anion transport activities is still the subject of much debate. At present, there are two main models for the mechanism of UCP-mediated proton conductance that have been proposed, each with several pieces of supporting evidence [23-28]. The fatty acid buffering hypothesis posits that UCP-mediated proton leak occurs via the protonation of fatty acid anions in the outer leaflet of the mitochondrial inner membrane, followed by their subsequent translocation to the inner leaflet via a flip-flop mechanism, deprotonation in the matrix, due to the change in pH across the membrane, and finally, export of the resulting fatty acid anions by the UCPs through an, as yet undetermined mechanism (figure 4B) [23, 26]. Alternatively, the fatty acid cofactor model proposes that the proton leak via the UCPs occurs through a mechanism in which the carboxyl groups on FFAs act as buffering cofactors in conjunction with proton conducting residues, such as the carboxylate groups of aspartate residues

(figure 4A) [23, 26]. However, recent evidence has called into question the validity of the fatty acid buffering hypothesis, in addition to certain aspects of the fatty acid cofactor model these include: the observation that UCP1-mediated respiratory uncoupling is activated by undecanesulfonate (C11S), despite the fact that the anionic group on C11S is highly acidic and therefore unable to accept a proton at physiologically relevant pHs and also, has been shown to be incapable of flip-flop between membrane leaflets; as well as observations from molecular modeling studies, which suggest that UCPs function in a channel like manner based on the presence of a funnel-like central pore that contains the nucleotide binding site in addition to two conserved, symmetrical salt bridges which could help facilitate substrate transport [27-29].

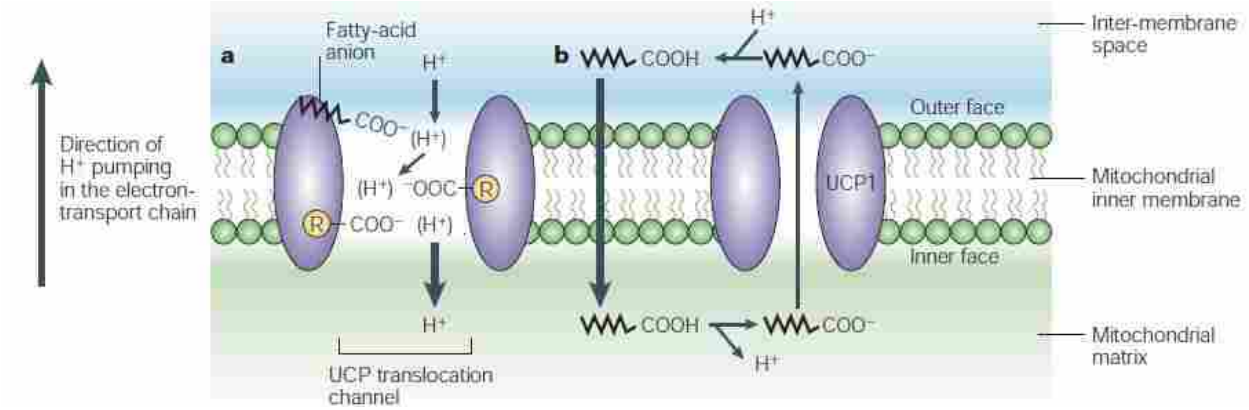

Figure 4: Diagram Representing Two of the Proposed Mechanisms for Proton Transport: (A) A diagram of the fatty acid cofactor model of proton transport by UCPs. In this model the fatty acids act as cofactors which provide additional carboxyl groups that accept protons from the intermembrane space and pass them on to proton buffering amino acids ($R\text{-}COO^-$) leading to translocation of protons into the matrix [23]. (B) A diagram depicting the fatty acid buffering model of proton transport by UCPs. In this model UCPs transport fatty acid anions from the matrix to the intermembrane space where they protonate, flip back to matrix side through a flip-flop mechanism and deprotonate into the matrix [23].

1.2.4 Uncoupling Protein 2

The second UCP that was identified, UCP2, has the widest tissue distribution of any of the UCP homologues, with near ubiquitous expression of its mRNA in mammals [9]. The wide tissue distribution of UCP2 mRNA expression has made it a particularly attractive target for research and has led to the observation that UCP2 may play a role in the pathological mechanisms of conditions such as chronic inflammatory diseases, obesity and type 2 diabetes [14,23,30-36]. Interestingly, despite its ubiquitous mRNA expression, the tissues in which detectable levels of UCP2 protein have been found are far more limited, suggesting that regulation of UCP2 expression may occur at both the transcriptional and translational levels [37,38]. For example, although the UCP2 mRNA is transcribed at high levels in spleen, heart, pancreatic β-cell, thymus, lung, macrophage, BAT and white adipose tissue, and in lower quantities in the brain, kidneys, liver and skeletal muscle, in tissue samples of BAT, skeletal muscle and heart no UCP2 protein could be detected [23,37]. In addition to its proposed role in several diseases, along with its widespread tissue distribution, UCP2 is also an attractive target for study, and will be the focus of the proposed work, because it has the highest sequence homology with UCP1 (59%) of any of the UCPs and should therefore share many of its previously determined structural and functional properties; it also has two highly conserved Trp residues, which are present in all 5 of the uncoupling protein homologues and whose usefulness as probes of protein structure and function will be the focal point of the next chapter (see figures 5 and 6) [28].

1.3 Research Objectives

Based on the properties of UCP2 outlined in the introductory chapter, the following research goals were planned for this study.

The first goal of the research project was to develop an expression system for efficient expression of UCP2 in bacterial membranes. This objective was achieved through removal of an endogenous NcoI restriction site from the cDNA sequence of UCP2 by silent mutation to allow for its introduction into an expression vector that was designed to express the protein in the bacterial cell membrane. The resulting plasmid with the *wt* UCP2 cDNA was then transformed into *E.coli* cells.

The second goal was to study the overall conformation and topology of UCP2 in membranes using biophysical spectroscopic techniques. To achieve this objective the only two Trp residues in UCP2, W178 and W283, were targetted. Overall, three Trp mutants of UCP2 cDNA were prepared, using the technique of overlap extension PCR. Two of these proteins were single mutants in which Trp was replaced by other aromatic residues, Phe or Tyr. The third protein was a double mutant version of UCP2 where the two Trp residues were replaced by Phe and Tyr. The resulting mutant cDNAs were introduced into the membrane-targeted expression vector and transformed into *E.coli* cells. Overexpressed *wt* UCP2 and the selective Trp mutants of UCP2, were then isolated, purified and verified by gel electrophoretic analytical techniques. The next step of this objective was to confirm that the selective Trp mutants of UCP2 retained native-like conformation using far-UV Circular Dichroism (CD) spectroscopy. The final step was to explore the local environment ot the Trps

in UCP2. For this purpose, fluorescence properties of Trp in *wt* UCP2 and each of its selective Trp mutants was characterized.

Several types of fluorescence assays were performed to complete the overall objective of the project, which was to examine the role of the conserved Trp residues that are present in all UCPs on their structure and proton transport activity, as well as to explore the overall membrane topology of UCP2 and the membrane topology of the nucleotide binding site of UCP2. These fluorescence based assays included SDS denaturation, acrylamide quenching, and proton transport assays.

The expected results, based on the limited structural information available for UCP2, were that the W176 residue would be found to be closer to the membrane interface than W283 residue, and the W283 residue was expected to be closer to the nucleotide binding site than the W176 residue. The Trp residues were not expected to directly play a role in proton transport by UCP2, but were expected to play some role in maintaining the native conformation of the protein. The introduced aromatic residue mutations were chosen to minimise change to the overall structure, and any changes in the conformation were expected to be in the local environment around each residue. This implies that despite similarity in overall conformation of the *wt* protein and its mutants, there may still be substantial differences in the proton transport activity of the proteins. Finally, it is expected that the selective Trp mutant with both Trp residues knocked out will have little to no fluorescence signal relative to the other UCP2 mutants and the *wt* protein. The details of the objectives of and

the techniques used in this study will be explained and discussed in the following chapters.

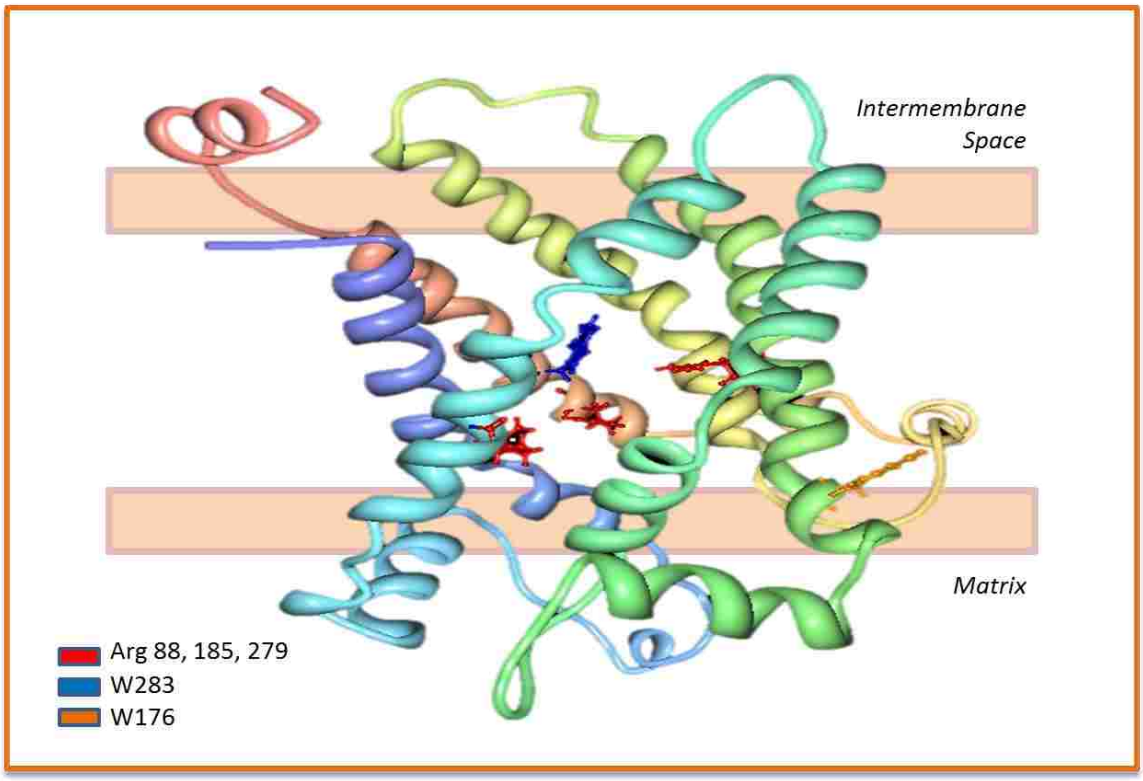

Figure 5: Model of UCP2 from NMR Fragment Searching with Trp Residues Visualised: A view of the model of the structure of UCP2, which has been proposed based on NMR fragment searching, with the tryptophan residues visualised in red and the arginine residues involved in nucleotide binding visualised in blue (W283) and orange (W176) [39].

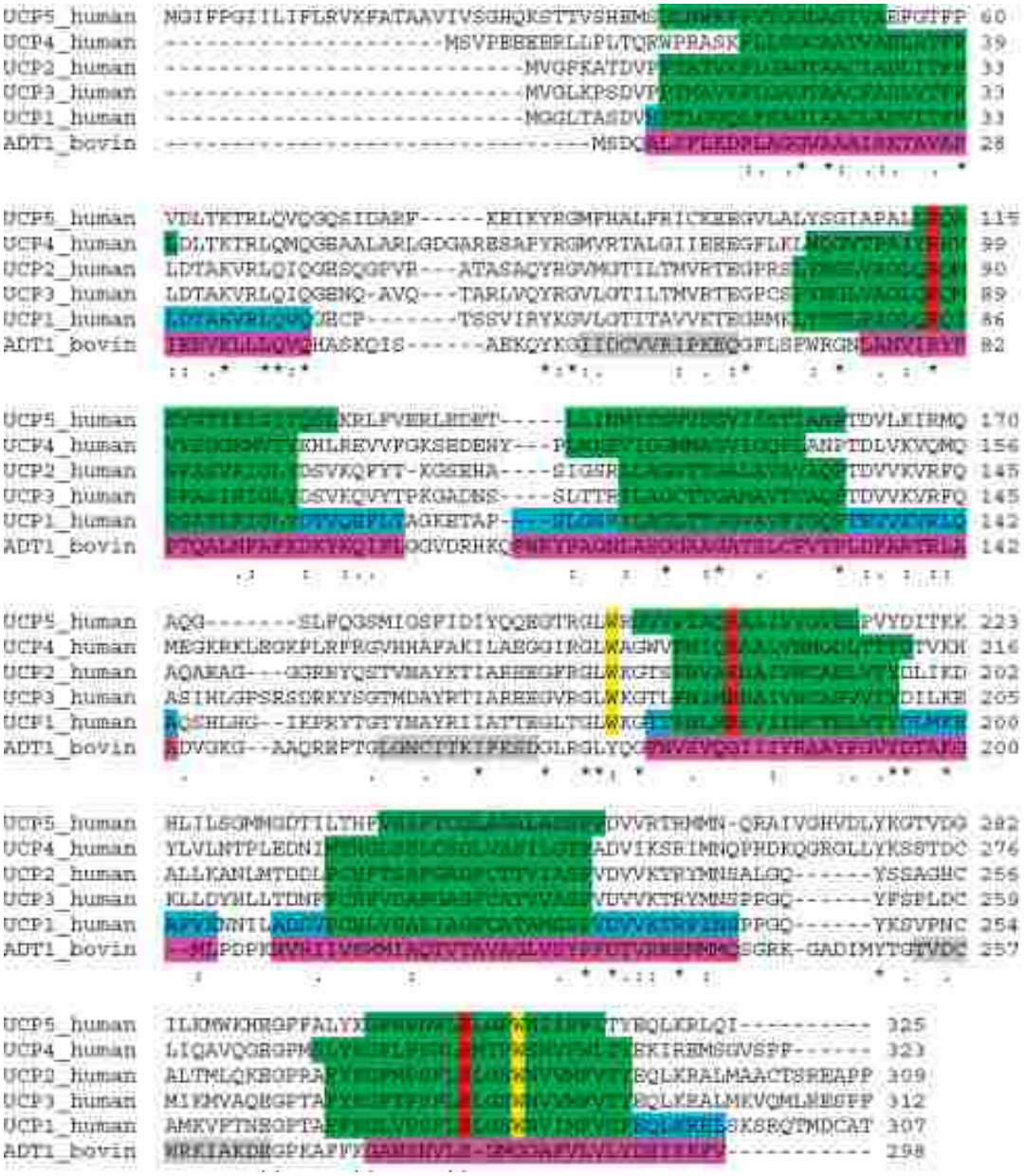

Figure 6: Sequence Alignment for the UCPs with ANT1: Sequence alignment of the human UCPs and bovine ANT1 based on the EBI Clustal W2 Multiple Sequence Alignment Tool and Swiss-Prot entries hUCP1 (P25874), hUCP2 (P558519), hUCP3 (P55916), hUCP4 (O95847), hUCP5 (O95258), and ANT1 (P02722) [41]. The positions of the two tryptophan residues are highlighted in yellow, the positions of the arginine residues involved in nucleotide binding are highlighted in red, transmembrane helices forming regions, as predicted by hydrophobicity scales are highlighted in green, the amphipathic helices of ANT1 are shown in grey and the known transmembrane helices of ANT1 are shown in magenta with the corresponding regions in UCP1 highlighted in light blue [40].

2 BIOPHYSICAL AND MOLECULAR BIOLOGY TECHNIQUES FOR STUDYING STRUCTURE AND FUNCTION OF MEMBRANE PROTEINS

2.1 The Use of Selective Trp Mutants of Membrane Proteins to Examine Folding, Membrane Topology and Enzymatic Activity

2.1.1 Site-Directed Mutagenesis by Overlap Extension PCR

In order to produce selective Trp mutants of UCP2, site-directed mutagenesis by primer overlap extension PCR was performed [43, 44]. This method of site-directed mutagenesis involves the introduction of a desired mutation into a gene of interest via three rounds of PCR with different combinations of four primers (outlined in figure 7). These four primers consist of: a forward flanking primer (primer A), which simply consists of the first ~15 base pairs of the sense strand of the gene of interest; a reverse primer (primer D), which is the reverse compliment to the 3' end of the sense strand and therefore simply copies the last ~15 base pairs of the antisense strand; the two remaining primers (Primers B and C) form a complementary pair approximately centred on the mutation one wishes to incorporate, if the mutation one wishes to incorporate is an addition or substitution these primers will simply consist of the added or swapped base pairs flanked by ~15 base pairs of the gene of interest's sense strand (primer B) or antisense strand (primer C) on both sides of where the desired mutation is to be incorporated. Once primers are designed and ordered, producing the gene of interest simply consists of three rounds of PCR as follows: round 1 with the original gene of interest as the

template and primers A and B as the forward and reverse primers, respectively; round 2 with the original gene of interest as the template and primers C and D as the forward and reverse primers, respectively; and a third round with the purified products of rounds 1 and 2 used as the template and primers A and D as the forward and reverse primers, respectively, yielding the gene of interest with the desired mutation added.

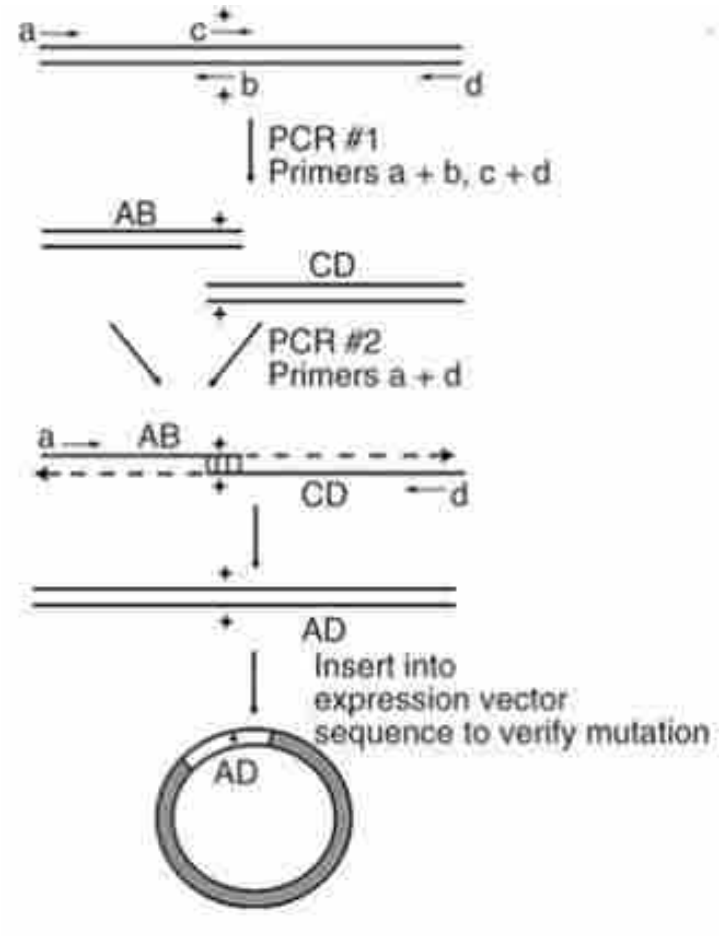

Figure 7: A Schematic Representation of Site-Directed Mutagenesis by Primer Overlap Extension PCR: A visual representation of the technique of site directed mutagenesis by primer overlap-extension PCR [44].

2.1.2 Examination of Protein Secondary Structure by Far-UV Circular Dichroism Spectroscopy

Plane polarised light can be thought of as being comprised of two circularly polarised components with equal magnitude. CD spectroscopy is based on the principle that when these circularly polarised components interact with a chiral molecule, the left handed and right handed components will be differentially absorbed, resulting in elliptical polarisation and as such data is usually reported in degrees of molar elipticity (see figure 8) [45]. When studying the secondary structure of proteins with CD spectroscopy, circularly polarised light in the 170-260nm region of the far-UV spectrum is typically used, in this region the primary chromophores are the amide bonds of the peptide backbone [45]. In secondary structure elements such as α-helices and β-sheets, the peptide chromophores are arranged in a very ordered way. The different orientations of the peptide bond chromophores in the various different types of secondary structure, result in shifts in the wavelengths that the chromophores absorb at, as well as changes in the intensity of absorption. Therefore, the CD spectra for each type of secondary structure is characteristic of that particular element and CD spectroscopy can be used to estimate the overall secondary structure composition of a protein (see figure 9)[46].

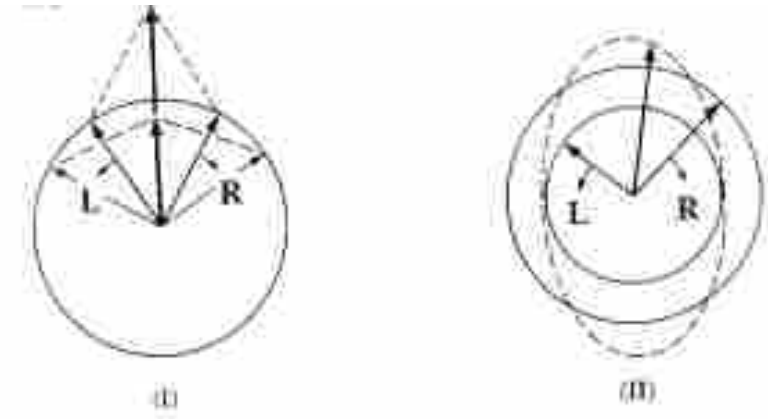

Figure 8: Depiction of Circular Dichroism: An illustration of the origin of elipticity arising from the differential absorption of left and right handed circularly polarised, also known as circular dichroism [46].

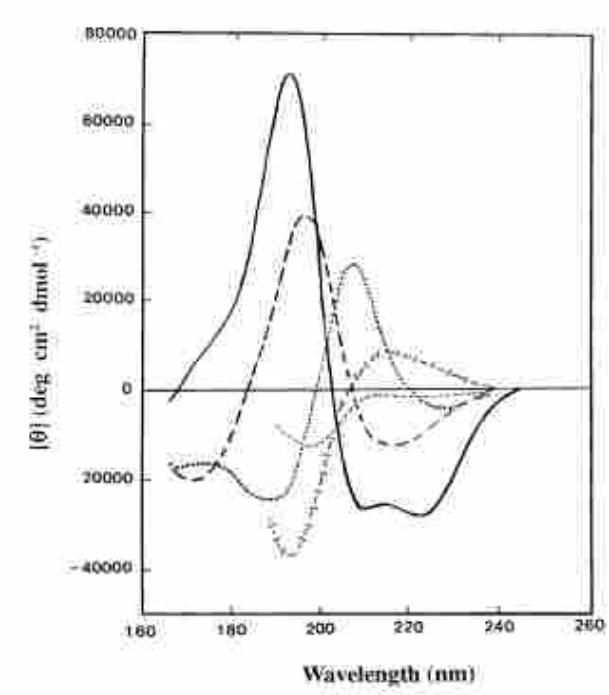

Figure 9: CD Spectra of Different Secondary Structure Elements: The Far UV CD spectra characteristic of various types of secondary structure. With the solid line sowing an, α-helix; the long dashed line an anti-parallel β-sheet; the dotted line a type I β-turn; the cross dashed line, an extended 31-helix or polyproline II helix; and the short dashed line, a disordered structure [46].

2.1.3 Fluorescence Based Spectroscopic Techniques for the Study of Proteins

One technique for probing the structure and function of proteins is fluorescence spectroscopy. One method of applying fluorescence spectroscopy to the study of proteins, involves taking advantage of the intrinsic fluorescence properties of the aromatic amino acids, namely tryptophan, tyrosine and phenylalanine. Of these amino acids, tryptophan is the fluorophore most commonly used in fluorescence spectroscopy, due the fact that it can be selectively excited and due to the sensitivity of its fluorescence to the polarity of the local environment around the residue [41]. Trp residues can be excited by UV light at 295nm, a wavelength at which the absorbance and resulting excitation of phenylalanine and tyrosine residues are insignificant. Trp residues that are excited at 295nm when fully exposed to a polar environment, such as water, have a resulting peak emission at around 350nm [41]. In contrast, due to the highly sensitive nature of the fluorescence of the residues to the polarity of their environment, a Trp residue that is excited at 295nm but is completely inaccessible to a polar solvent, such as a residue buried in the hydrophobic core of the protein or the membrane embedded domain of an integral membrane protein, will have a resulting peak emission that is blue-shifted down to around 300nm and a more structured emission spectrum, in that the slight shoulder present in the longer wavelengths of the absorption spectrum of tryptophan will become apparent in the emission spectrum [41]. Therefore, due to the selective and sensitive nature of Trp fluorescence, changes in the emission spectra of a protein that is excited at 295nm in response to, for instance, the addition of a possible

ligand, can be used to make inferences about properties of the protein, such as conformational changes in response to binding or the mechanism of action [41].

Fluorescence quenching is a widely applied technique that is used to assess the accessibility of a fluorophore (Trp), to a quenching agent [41]. There are two main types of quenching, static and dynamic. In static quenching, the quenching of fluorescence occurs via the formation of a complex between the fluorophore and the quenching agent in the ground state. In contrast, dynamic quenching occurs through the transfer of energy from an excited state fluorophore to a quenching agent through several different mechanisms, with the most relevant to the study of proteins being direct collisional energy transfer [41,42]. As the name suggests, collisional energy transfer involves the transfer of energy through direct collisions between the excited state fluorophore and the quenching agent resulting in a relaxation of the excited state of the fluorophore without the emission of photons [42]. The quenching agents commonly used for collisional quenching mostly consist of small, polar molecules such as acrylamide, iodide and molecular oxygen [42]. Site-directed mutagenesis to produce selective tryptophan mutants of a protein is a method that is sometimes used to compliment the study of proteins via their intrinsic fluorescence and fluorescence quenching, by allowing the local environment of each individual Trp residue in a given protein, to be probed separately, which removes the need for trying to assign specific aspects of changes in the spectra to certain Trp residues [41].

2.1.3.1 Spectral Properties of Proteogenic Amino Acids

Phenylalanine, tyrosine and tryptophan are the three aromatic amino acids found in proteins. All three of these aromatic amino acids possess the ability to act as intrinsic fluorophores within proteins. Of the three, Phe has the weakest fluorescence by a large margin, followed by Tyr which had moderate fluorescence and finally Trp, which the highest quantum yield relative to the other aromatic amino acids [39]. Figure 10 shows the general absorption and emission spectra for each of the three aromatic amino acids found in proteins, from this it can be seen that Trp residues have an absorption spectrum that extends to just past 300nm and that at 295nm Trp still has significant absorbance, whereas Phe and Tyr do not. The presence of this range of wavelengths, where Trp residues absorb photons and the other aromatic residues do not, means that the fluorescence of Trp residues can be selectively excited at these wavelengths without appreciable fluorescence from Tyr or Phe residues [41]. Another interesting property of Trp residues is that they are highly sensitive to the polarity and pH of the local environment around the residues with a significant blue shift coupled with an increase in fluorescence intensity when in a nonpolar versus a polar environment, respectively. This sensitivity to the environment around the Trp residues is not seen in the other aromatic amino acids, which are fairly insensitive to changes in their local environments [41].

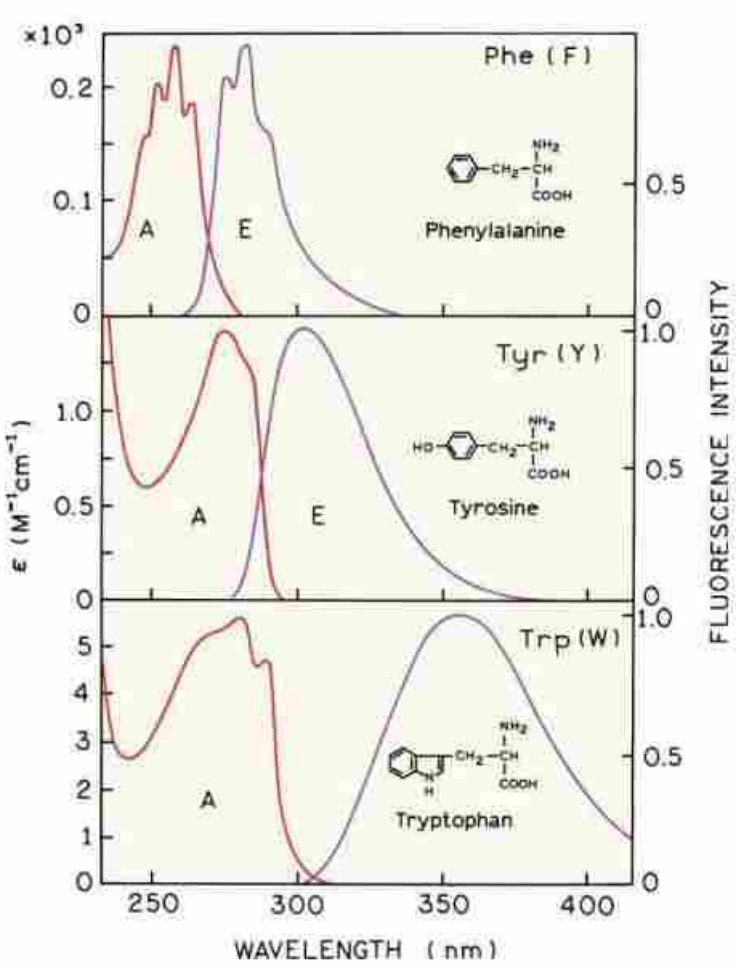

Figure 10: Absorbance and Emission Spectra of the Aromatic Amino Acids: The general absorption and emission spectra for each of the three aromatic amino acids found in proteins. The spectra on the left in (red) show the absorbance profiles of the amino acids and the spectra on the right (purple) show the emission profiles of each amino acid. Figure was retrieved from [41].

2.1.3.2 Intrinsic Fluorescence of Trp Containing Proteins

The sensitivity of Trp fluorescence to the environment surrounding the residue, as well as the fact that Trp residues can be selectively excited at 295nm, as discussed above, give rise to the possibility of using the residue as a fluorescent

probe of structure. This application is especially useful for studying membrane proteins, for which structural information is usually difficult to obtain by other methods such as X-ray crystallography [41,47.] As a logical extension of the aforementioned fluorescence properties, the wavelength of emission, as well as the quantum yield of fluorescence, can give information about the relative position of a Trp residue in a protein that is folded in a membrane, with membrane buried Trp residues having lower wavelengths of emission (blue-shifted) and higher quantum yields relative to those of solvent exposed Trp residues. Therefore fluorescence spectroscopy of proteins with excitation at 295nm can yield information about the overall topology of integral membrane proteins, especially when applied to selective Trp mutants, which contain only a single Trp residue, thus allowing the fluorescence signal obtained to be related solely to that residue [41, 42].

2.1.3.3 Quenching of Trp Fluorescence

Fluorescence quenching is a widely used technique that has been in use since the 1960s. The technique is used to determine the accessibility of fluorophores, such as Trp in proteins, to a quenching agent [42, 48]. These quenching agents are usually polar molecules or ions dissolved in the solvent. As such, the fluorescence of Trp residues on the surface of a cytosolic protein and those at the membrane-solvent interface of membrane proteins will experience the greatest degree of fluorescence quenching. Conversely, if the Trp residues are buried in the hydrophobic core of a protein, or embedded within the membrane, they have their fluorescence quenched to a lesser extent due to decreased accessibility to the quenching agent [42]. This can yield topological information on the protein being

studied as well as information on structural changes in response to ligand binding. Some common quenchers used in the study of biomolecules are shown in table 1 [41].

Table 1: Assorted Quenchers and their Corresponding Fluorophores: Common quenchers used for fluorescence quenching studies and the fluorophore they quench. Table was obtained from [41].

Quenchers	Typical fluorophore	References
Acrylamide	Tryptophan, pyrene, and other fluorophores	5–7, 176–180
Amines	Anthracene, perylene	2, 124, 181–186
Amines	Carbazole	187
Amine anesthetics	Perylene, anthroyloxy probes	188–190
Bromate	–	191
Bromobenzene	Many fluorophores	192
Carbon disulfide	Laser dyes, perylene	193
Carboxy groups	Indole	194
Cesium (Cs^+)	Indole	195
Chlorinated compounds	Indoles and carbazoles	196–199
Chloride	Quinolinium, SPQ	200–203
Cobalt (Co^{2+})	NBD, PPO, Perylene (Energy transfer for some probes)	204–210
Dimethylformamide	Indole	211
Disulfides	Tyrosine	212
Ethers	9-Arylxanthyl cations	213
Halogens	Anthracene, naphthalene, carbazole	214–229
Halogen anesthetics	Pyrene, tryptophan	230–232
Hydrogen peroxide	Tryptophan	233
Iodide	Anthracene	234–237
Imidazole, histidine	Tryptophan	238
Indole	Anthracene, pyrene, cyanoanthracene	239–241
Methylmercuric chloride	Carbazole, pyrene	242
Nickel (Ni^{2+})	Perylene	243–244
Nitromethane and nitro compounds	Polycyclic aromatic hydrocarbon	245–256
Nitroxides	Naphthalene, PAH, Tb^{3+}, anthroyloxy probes	257–266
NO (nitric oxide)	Naphthalene, pyrene	267–270
Olefins	Cyanonaphthalene, 2,3-dimethylnaphthalene, pyrene	271–273
Oxygen	Most fluorophores	274–290
Peroxides	Dimethylnaphthalene	291
Picolinium nicotinamide	Tryptophan, PAH	292–296
Pyridine	Carbazole	297
Silver (Ag^+)	Perylene	298
Succinimide	Tryptophan	299–300
Sulfur dioxide	Rhodamine B	301
Thallium (Tl^+)	Naphthylamine sulfonic acid	302
Thiocyanate	Anthracene, 5,6-benzoquinoline	303–304
Xenon		305

3 MATERIALS, EXPERIMENTAL DESIGN AND METHODS

3.1 Materials

Primers were ordered from Life Technologies, a Thermo Fisher Subsidiary (Massachusetts, USA); the Wizard Plus SV Miniprep DNA Purification System and Wizard SV Gel and PCR Clean-Up System were from Promega (Wisconsin, USA.); HotStar HiFidelity DNA polymerase kit was from Qiagen (Germany); DNA sequencing was performed at The Centre For Applied Genomics (TCAG) (Ontario, Canada). All other chemicals used for the PCR and subsequent cloning into pET26b(+) and transformation into *E.coli* were order from either BioShop Canada Inc. (Ontario, Canada) or Thermo Fisher (Massachusetts, USA).

n-Octyl-β-D-Glucopyranoside (OG) was obtained from Anatrace (California, USA); Nickel-NTA beads were obtained from Qiagen (Germany); Tris(hydroxypropyl)phosphine (THP) was obtained from EMD Milipore (Massachusetts, USA); acrylamide monomer (no bis-acrylamide) was obtained in powder from BioShop Canada Inc. (Ontario, Canada); L-α-Lecithin, composed of a minimum 60% phosphatidylcholine with the other 40% primarily comprised of phosphatidylethanolamine with small amounts of cholesterol and triglycerides, was obtained from Sigma-Aldrich (Missouri, USA); SPQ fluorophore was obtained from Biotium Inc. (California, USA); ATP and sodium palmitate were also purchased from Sigma-Aldrich (Missouri, USA); SM-2 Biobeads were obtained from Bio-Rad (California, USA); Sephadex G25-300 (Coarse) were obtained from GE Healthcare

(United Kingdom). Valinomycin and Nigericin were purchased from Sigma-Aldrich (Missouri, USA) and stored in 100% ethanol at -40°C; all centrifugation took place in Beckman-Coulter (California, USA) rotors and centrifuges unless otherwise noted. All other chemicals used in the fluorescence assays of UCP2 were either purchased from BioShop Canada Inc. (Ontario, Canada) or VWR (Pennsylvania, USA).

3.2 Experimental Design and Methods

3.2.1 Site-Directed Mutagenesis by Primer Overlap Extension PCR and Cloning into the Bacterial Membrane-Targeting pET26b(+) Vector

The first objective of this project was to clone N-terminally His-tagged *wt UCP2* into the pET26b(+) vector. In order to accomplish this, N-terminally His-tagged *wt UCP2-pET21d* was used as a template, and two gene flanking primers were designed for site-directed mutagenesis by overlap-extension PCR by choosing a sequence, ~30bp long, on opposite strands at either end of the wild type (wt) hUCP2 gene, with the forward flanking primer containing the His-tag sequence as well as an NcoI site at the 5' end and the reverse primer containing a HindIII restriction site downstream of the coding sequence (see appendix 1 for a full list of the primers used). A pair of mutagenic primers was also designed to introduce a single base pair change in order to knock out an endogenous NcoI site in *UCP2* without altering the translated sequence. This was accomplished by copying ~15 nucleotides from either side of the endogenous NcoI site and knocking it out by changing the CCATGG recognition site to CTATGG. *wt UCP2-pET21* in DH5α *E.coli* was used to inoculate a 10mL stock of Luria-Bertani (L.B.) broth containing

50µg/mL of ampicillin in a 15mL falcon tube. The inoculated culture was then loosely capped and grown at 37°C with 240 RPM of horizontal shaking in a shaking incubator for 18h. The cells were subsequently spun down in a clinical centrifuge at 4000xg for 10 minutes and plasmid was isolated using the Wizard Plus SV Miniprep DNA Purification System (Promega), according to the available protocol and then used as a template for amplification and mutagenesis to yield the desired Trp mutations [49]. To produce the N-terminally His-tagged *UCP2* with the endogenous NcoI site knocked out and with the 5'NcoI site added, the NcoI knockout mutagenic primer set was used, and primer overlap extension PCR was performed. All PCR was performed using the *HotStar HiFidelity Polymerase Kit* (Qiagen) and all reactions were set up in dome capped PCR tubes as outlined in table 2. The PCR tubes were subsequently placed in a thermocycler and cycled using the conditions outlined in table 3. The resulting PCR products were then run on a 1% agarose gel at 120V for 1 hour with a 1kb ladder and imaged using the *VersaDoc 4000 Gel Imaging System* (Bio-Rad) in order to confirm that DNA bands of the expected length were produced. Following confirmation of the presence of PCR products of the expected lengths for the first two rounds of PCR, a third round of PCR was performed yielding the ~1kb N-terminally His-tagged *UCP2* with a 5'NcoI restriction site added and the endogenous *UCP2* NcoI site knocked out.

Following the amplification and mutagenesis of *UCP2*, the next goal was to clone the *wt UCP2* into the pET26b(+) expression vector, which contains a pelB leader sequence that allows for targeting of an expressed gene product to the bacterial membrane. The *UCP2* NcoI knockout produced by PCR was purified by gel

purification using the *SV gel and PCR Cleanup kit* (Promega) according to the kit protocol [50]. Next, 1.5µg of each PCR product and 1.5µg of empty pET26b(+) vector were subjected to a double restriction digest, with *NcoI-HF* and *HindIII-HF* from NEB, at 37°C for 3 hours in *CutSmart Buffer* (New England Biolabs). The products of the double digests were then gel purified as described above for the PCR products. Each of the mutant hUCP2 genes were then ligated into pET26b(+) vectors. The ligation reactions consisted of 50ng of the restriction digested pET26b(+) vector and ~200-300ng of a digested hUCP2 mutant gene, with 1µL *T4 DNA ligase*. The ligation reactions were incubated at 16^0C for 14h. The *UCP2-pET26b(+)*was then used to transform DH5α and BL21 (DE3) RIPL *E.coli* cells (hereafter referred to as BL21 CD^+), as described in the following section.

Two additional sets of mutagenic primers were subsequently designed with the aim of producing three selective Trp mutants of UCP2 in a pET26b(+) expression vector (W176Y, W283F and W176Y-W283F), using the newly produced *wt UCP2-pET26b(+)* construct as a template. This was achieved by again using primer overlap-extension PCR with same flanking primers used for amplifying *wt UCP2* from the pET21d vector. Four additional primers were designed to introduce the desired mutations into the hUCP2 gene. These primers consisted of two complementary pairs, one to introduce the W176Y mutation and the other to introduce the W283F mutation. The primers for the W176Y mutation were designed by copying a ~15bp sequence on both sides of the Trp codon at position 176, for the sense strand primer (primer C1) the TGG Trp codon was replaced with a TAC Tyr codon and for the antisense strand primer (primer B1) the CCA bases were replaced

with GTA. The primers for the *W283F* mutation were designed by again copying a ~15bp sequence on both sides of the trp codon, this time at position 283, for the sense strand primer (primer C2) the TGG Trp codon was replaced with a TTC Phe codon and for the antisense strand primer (primer B2) the CCA bases were replaced with TTC. To introduce the *W176Y-W283F* mutation into the hUCP2 gene both the *W176Y* primers and the *W283F* primers will be used as described below (see appendix 1 for a full list of the primers used).

wt UCP2-pET26b(+) plasmid was isolated used as a template for amplification and mutagenesis to yield the desired Trp mutations [49]. To produce the W176Y and W283F mutations, mutagenic primer sets 1 and 2 were used, respectively, and primer overlap extension PCR was performed. All PCR was performed using the *HotStar HiFidelity Polymerase Kit* (Qiagen) and all reactions were set up in dome capped PCR tubes as outlined in table 4 [51]. The PCR tubes were subsequently placed in a thermocycler and cycled using the conditions outlined in table 3. The resulting PCR products were then run on a 1% agarose gel at 120V for 1 hour with a 1kb ladder and imaged using the Bio-Rad VersaDoc 4000 Gel Imaging System in order to confirm that of DNA bands of the expected length were produced. Following confirmation of the presence of PCR products of the expected lengths for the first two rounds of PCR, a third round of PCR was performed yielding each of the ~1kb single Trp mutants (W176Y and W283F). In order to produce the double Trp mutant (W176Y-W283F) the W176Y product was then gel purified, as described above, and then used as a template for the first two rounds of primer-overlap

extension PCR with the W283F primers, and cycled under the conditions outlined in table 3.

Following the amplification and mutagenesis of *UCP2*, the next goal was to clone the *UCP2* Trp mutants into the pET26b(+) expression vector. In order to clone the desired *UCP2* inserts into the pET26b(+) vector, a glycerol stock of empty pET26b(+) vector in DH5α *E.coli* was used to grow up a 10mL as described previously for *UCP2-pET21* but with the ampicillin replaced by 50μg/mL of kanamycin (kan). Plasmid was again isolated from the overnight culture using the Wizard Plus SV Miniprep DNA Purification system (Promega) [49]. After isolating the plasmid the UCP2 Trp mutant genes produced by PCR were purified by gel purification using the Promega SV gel and PCR Cleanup kit according to the kit protocol [50]. The 1.5μg of each PCR product and 1.5μg of empty pET26b(+) vector were then subjected to a double restriction digest, with *NcoI-HF* and *HindIII-HF* from NEB, at 37°C for 3 hours in CutSmart Buffer. The products of the double digests were then gel purified as described above for the PCR products. Each of the mutant hUCP2 genes were then ligated into pET26b(+) vectors. The ligation reactions consisted of 50ng of the restriction digested pET26b(+) vector and ~200-300ng of a digested hUCP2 mutant gene, with 1μL *T4 DNA ligase*. The ligation reactions were incubated at 16^0C for 14h.

Table 2: PCR Reaction Setup for NcoI Knockout/Addition for wt UCP2: Volumes of each component for overlap-extension PCR reactions used to produce UCP2 with its endogenous NcoI restriction site removed by the silent mutation of a single nucleotide and an NcoI restriction site added immediately adjacent to the gene on the 5' end, as well as a HindIII site on the 3' end.

	PCR Rounds 1 and 2 (Single Mutants)	**PCR Round 3**
5X HotStar HiFidelity PCR Buffer	10µL	10µL
HotStar HiFidelity DNA Polymerase	1µL	1µL
Forward Primer (100µM in H_2O)	0.5µL	0.5µL
Reverse Primer (100µM in H_2O)	0.5µL	0.5µL
Template DNA (50-100ng/µL)	1µL Isolated *UCP2-pET21*	1µL Purified Round 1 PCR Product + 1µL Purified Round 2 PCR Product
Nuclease Free H_2O	37µL	37µL
Total Reaction Volume	50µL	50µL

Table 3: Cycling Conditions Used for PCR Reactions: Thermocycler conditions used for all overlap-extension PCR reactions.

Cycling Steps (Number of Cycles)		PCR Rounds 1 and 2	PCR Round 3
Activation (1X)	Temperature (°C)	95	95
	Time per cycle (s)	300	300
Denaturation (40X)	Temperature (°C)	94	94
	Time per cycle (s)	15	15
Annealing (40X)	Temperature (°C)	59	59
	Time per cycle (s)	30	30
Extension (40X)	Temperature (°C)	72	72
	Time per cycle (s)	30	60
Final Extension (1X)	Temperature (°C)	72	72
	Time per cycle (s)	600	600

Table 4: PCR Reaction Setup for Site-Directed Mutagenesis of Trp Residues in UCP2: Volumes of each component for overlap-extension PCR reactions used to produce the three previously described selective Trp mutants of UCP2.

	PCR Rounds 1 and 2 (Single Mutants)	**PCR Round 3**
5X HotStar HiFidelity PCR Buffer	10µL	10µL
HotStar HiFidelity DNA Polymerase	1µL	1µL
Forward Primer (100µM in H_2O)	0.5µL	0.5µL
Reverse Primer (100µM in H_2O)	0.5µL	0.5µL
Template DNA (50-100ng/µL)	1µL Isolated *UCP2-pET26b(+)* *(W176Y and W283F)* *Or* 1µL W176Y-pET26b(+) (*W176Y-W283F*)	1µL Purified Round 1 PCR Product + 1µL Purified Round 2 PCR Product
Nuclease Free H_2O	37µL	37µL
Total Reaction Volume	50µL	50µL

3.2.2 Transformation of DH5α and BL21 Codon Plus *E.coli* with hUCP2 Trp Mutants in pET26b(+) Vector

Each of the cloned UCP2 Trp mutant vectors was then used to transform chemically competent DH5α E.coli cells. This was done by adding ~100ng of vector

to 100μL aliquots of competent DH5α E.coli cells and then incubating on ice for 30 min, which was then followed by heat shock at 42^0C for 90s. After the heat shock the cells were placed back on ice for 30 min. The cell aliquots were diluted to 900μL with LB broth and incubated at 37^0C for 1h. After this incubation, 100μL aliquots of the cultures were plated onto LB-Agar plates containing 50μg/mL of kan. These plates were inverted and incubated at 37^0C overnight.

Following the overnight incubation, colonies were selected from the plates and the success of the transformation was evaluated by colony PCR. Colony PCR reactions were prepared with 1.8μL 10x thermo Pol buffer, 0.36μL 1mM deoxynucleotide triphosphate mixture, 0.5μL 100μM primer A, 0.5μL 100μM primer D, 0.09μL Taq DNA polymerase and 11.75μL nuclease free H_2O. Each PCR reaction was then inoculated with one of the colonies selected from the agar plates used in the transformation reaction. The PCR reaction mixtures was then placed in a thermocycler, and cycled under the following conditions: 5 minutes at 95^0C for the initial activation, followed by 30 repeats of the cycle 15s of denaturation at 94^0C, 30s of annealing at 58^0C and 1 minute of extension at 72^0C. The PCR reaction again ended with a final extension step of 10 minutes at 72^0C. The results of the colony PCR were analysed by agarose gel electrophoresis on a 0.8% agarose gel, stained with ethidium bromide.

Glycerol stocks were prepared for colonies confirmed to contain the mutant hUCP2 gene insert (1 for each mutation). This involved growing up 4mL overnight cultures, containing 50μg/mL Kan, for each colony that was selected. 0.7mL from

each culture was then mixed with 1.3mL 50% glycerol, in a 2mL tube and these were stored at -80^{0}C until used. Plasmid isolation was performed on each of the mutants as described for pET26b(+) in the above section and samples of the plasmid were sent to The Centre for Applied Genomics (TCAG) (The Hospital for Sick Children, Toronto, ON) for DNA sequencing. All plasmid samples sent for sequencing had the sense and anti-sense strands of the insert region sequenced with a T7 promoter primer and a T7 terminator primer, respectively.

The isolated plasmid was then transformed into BL21 CD$^+$, using the same procedure as was used for the DH5α transformation with the addition of 25μg/mL streptomycin (strep) and 25μg/mL of chloramphenicol (cam) to the selective agar plates.

3.2.3 Membrane Targeted Expression of hUCP2 Mutants from BL21 Codon Plus

Following verification of the presence of the desired UCP2 inserts in pET26b(+) by DNA sequencing, recombinant wt UCP2, as well as each of the UCP2 Trp mutants, were overexpressed in BL21 CD$^+$. Overexpression of wt UCP2 and the three Trp mutants was achieved using the autoinduction method [52]. This was done by preparing 930mL of ZY media by dissolving 10g of Tryptone and 5g of yeast extract in a 2800mL Fernbach culture flask and then sterilizing by autoclaving on a liquid cycle with a 30min sterilization time. The sterile media was then allowed to cool to room temperature overnight. The same day the ZY media was prepared an overnight culture was prepared under aseptic conditions, consisting of 20mL of L.B. broth in a 50mL falcon tube with 50μg/mL kan, 25μg/mL cam and 25μg/mL strep.

The overnight culture was then inoculated with the BL21 CD^+ glycerol stock containing the desired UCP2-pET26b(+) construct and placed in a shaking incubator at 37°C with 240RPM shaking for 18h. Immediately prior to the end of the overnight incubation the ZY media was prepared for autoinduction via the addition of 1mL of 1M $MgSO_4$ followed by the addition of 50mL and 20mL of 20X NPS (0.5M $(NH_4)_2SO_4$, 1M KH_2PO_4, 1M Na_2HPO_4), and 50X5052 (25% glycerol (w/v) 2.5% glucose and 10% lactose) respectively. Finally, kan, cam and strep were added, followed by the 20mL overnight culture, yielding a final culture volume of 1L containing 1% Tryptone, 0.5% yeast extract, 1mM $MgSO_4$, $(NH_4)_2SO_4$, 50mM KH_2PO_4, 50mM Na_2HPO_4, 0.5%glycerol (w/v), 0.05% glucose, 0.2% lactose, 50µg/mL kan, 25µg/mL cam and 25µg/mL strep. The now fully prepared and inoculated autoinduction media was then placed in a shaking incubator and grown at 22°C with 250RPM of shaking for 22h. The culture was split into centrifuge tubes and cells were collected by centrifuging at 8000xg for 15min at 4°C and then decanting the supernatant and transferring to a 50mL Falcon tube. The cell pellets were then stored at -20°C until used in the cell lysis experiment described below.

3.2.4 Cell Lysis, Membrane Isolation, and Purification of Expressed UCP2 by IMAC

In order to extract and purify the desired UCP2 mutant proteins from the cell pellets they were thawed on ice and then resuspended in 50mL Extraction Buffer (E.B.) containing 20mM Tris-HCl, 0.5M NaCl, 0.5mg/mL DNase, 0.2mg/mL lysozyme and 1 *c0mplete protease inhibitor cocktail* tablet (Roche Applied Science), pH8.0. The resuspended cells were then incubated at 4°C for 20min to allow time for lysozyme digestion. Subsequently, the cells were loaded into the *Constant Cell Distribution*

System Model T2/40/BA/AA (Constant Systems) and passed through three times at 20000p.s.i. The cell lysate was cleared of cellular debris and unbroken cells by centrifuging at 20000xg for 20min and then collecting the supernatant and discarding the pellet. The cell lysate was subjected to ultracentrifugation at 50000RPM for 1h in a *Optima™ Max* ultracentrifuge (Beckman-Coulter) using an *MLA80* rotor (Beckman-Coulter) to pellet the bacterial membranes. The supernatant was discarded and the pellets were fully resuspended in 30mL of Binding Buffer (B.B.) (20mM Tris-HCl, 0.5M NaCl, 1% N,N-dimethyldodecylamine-N-oxide also known as Lauryldimethylamine-oxide (LDAO), 20mM Imidazole and 1mM THP, pH8.0) by passing back and forth through a 20 gauge needle attached to a 5mL syringe and then transferring to a 25mL Erlenmeyer Flask with a stir bar at 4°C on a stir plate for 2h. At that point, any remaining insoluble particles were removed from the sample by a final centrifugation at 10000xg for 10min at 4°C. Concurrently, an immobilized metal affinity chromatography (IMAC) gravity column containing ~4mL of nickel-nitrilo-triacetic acid-Agarose beads (Ni-NTA-Agarose) (Qiagen) was prepared and equilibrated with 2 passes of 20mL of B.B. Following the final centrifugation the resuspended membrane, containing the overexpressed recombinant UCP2, was loaded onto the equilibrated IMAC column, the flow rate was set to ~1mL/min and the entire sample was passed through the column 3 times to allow for binding of the recombinant His-tagged UCP2 before the flow through was discarded [53]. The column was then washed with two passes of 20mL of Wash Buffer (20mM Tris-HCl, 0.5M NaCl, 1% Octyl-Glucoside (OG), 40mM imidazole and 1mM THP, pH8.0), after which the bound protein was eluted using elution buffer

(20mM Tris-HCl, 0.5M NaCl, 1% Octyl-Glucoside (OG), 400mM imidazole 1mM THP, pH8.0) and ten 1mL fractions were collected . The concentration of protein in each collected fraction was then determined by Bradford assay using *Bio-Rad Protein Assay Dye Reagent Concentrate* (Bio-Rad) with a Bovine Serum Albumin (BSA) standard and the three most concentrated fractions were pooled [53]. The pooled fractions were afterwards exchanged into either desalt buffer (D.B.) (20mM Tris-HCl, 50mM NaCl, 1% glycerol and 1% OG, pH8.0) or, if the isolated protein was to be reconstituted for the purposes of assaying its proton transport activity, 1.5X Proton Transport Internal Buffer (I.B.) (1x I.B.: 30mM [tris(hydroxymethyl)methyl]-2-aminoethanesulfonic acid (TES) buffer, 80mM tetraethylammonium sulfate ($(TEA)_2SO_4$), and 1mM EDTA, pH7.2) using an *Econo-Pac®10DG Desalting Prepacked Column* according to the available general protocol [55] The isolated and purified recombinant UCP2 was then stored at -80^{0}C until ready to be used, for protein stored in 1.5X I.B. this was a maximum of 18h. Purity of the protein samples obtained were assessed by SDS-PAGE stained with Coomassie blue. A second unstained SDS-PAGE gel was run and subsequently transferred to nitrocellulose using a semi-dry transfer, blocked overnight in 5%(w/v) skim milk powder in tris buffered saline with tween buffer (TBS-T) (10mM Tris-HCl, 150mM NaCl, 0.05%(w/v) Tween 20, pH7.5) and the isolation of the target protein was verified by a Western blot that was developed using an anti-His primary antibody from a mouse host (Rockland Immunochemicals) and an anti-mouse/horseradish peroxidase conjugated secondary antibody from a rabbit host (Rockland Immunochemicals). A second Western blot was then performed, in order to definitively establish the

presence of UCP2 in the sample, using the same method just described but with the mouse anti-his primary antibody replaced by an anti-UCP1 primary antibody that was also from a rabbit host (Rockland Immunochemicals) and with the secondary antibody replaced by anti-rabbit/horseradish peroxidase conjugated secondary antibody from a goat host (Rockland Immunochemicals).

3.2.5 Circular Dichroism Spectroscopy of Selective Trp Mutants of UCP2

After confirming that the desired UCP2 Trp mutants, as well as wt UCP2, were successfully produced, isolated and purified, the conformational equivalence of the mutants was confirmed by C.D. spectroscopy. To this end, purified stocks of wt UCP2 and each of the selective Trp mutants of UCP2 were retrieved from the -80°C freezer and allowed to thaw on ice. Once fully thawed, a Bradford assay was performed, as described in previous sections, to determine the molar protein concentration in each stock. The stocks of protein used for C.D. spectroscopy experiments were then diluted to 8μM with D.B. Samples of each protein were then loaded into a clean quartz cell with a 0.1nm path length and far-UV C.D. measurements were obtained by scanning in *Aviv 215 spectropolarimeter* (Aviv Biomedical) at 25°C. All included spectra are the average of eight scans.

3.2.6 Intrinsic Fluorescence Assays for Selective Trp Mutants of UCP2

3.2.6.1 Sample Preparation or Intrinsic Fluorescence Measurements

After conformational equivalence of the selective Trp mutants of UCP2 was confirmed, with respect to the wt, the intrinsic fluorescence of each of the three selective Trp mutants of UCP2, as well as the wt, was next assessed. To do this, the

purified stocks of wt UCP2 and the UCP2 Trp mutants in D.B. were retrieved from the -80^{0}C freezer and allowed to thaw on ice. Once the stocks were fully thawed a Bradford assay was performed using *Bio-Rad Protein Assay Dye Reagent Concentrate* (Bio-Rad) and BSA standards. Next, 4μM working stocks of each of the proteins were then made by diluting each with the required amount of D.B. and a Bradford was again performed as described above. The 4μM working stocks were then used to make as many 1mL 1μM samples as the following fluorescence assays required.

3.2.6.2 Intrinsic Fluorescence Measurements

To perform the desired intrinsic fluorescence measurements, 800μL of 1μM sample for each of the three UCP2 selective Trp mutants were obtained and total fluorescence and Trp fluorescence spectra from 200nm to 600nm were obtained by scanning with 280nm and 295nm excitation wavelengths, respectively. All scans were performed in a quartz cuvette with a 1cm pathlength (Hellma Analytics) using a *Cary® Eclipse* spectrofluorometer (Varian) with a scan rate of 600nm/min, the excitation slit width set to 5nm and detector voltage set to 800V. Between samples the cuvette was washed thoroughly with methanol, followed by ultrapure water and finally methanol again before it was dried under a 99.998% pure N_2 gas stream. Blank samples containing only D.B. were also scanned under the same conditions. After the UCP2 samples were scanned another Bradford assay was performed, as described previously so that the fluorescence signals could later be standardized with respect to the micromolar concentration of protein in each sample. The spectra resulting from the blank scans were then subtracted from the protein sample scans

and the baseline-corrected spectrum for each of the UCP2 samples was subsequently standardized by dividing by its respective micromolar concentration.

3.2.6.3 SDS Denaturation Assay

The effect of SDS denaturation on the Trp fluorescence spectrum of UCP2 was next assayed, as was the effect of binding a known ligand, ATP, on said denaturation. To accomplish this, four sets of samples were prepared for each of the UCP2 Trp mutants and the wt UCP2, as described in section 3.2.5.2, as well as four blanks, containing only D.B. One set of UCP2 samples and one blank were scanned as described in the preceding section. Next, 20mM of SDS from a 693mM stock was added to each of the second set of samples and blank and these were again scanned using the conditions outlined in the preceding section. Following these scans, 50μM ATP was added to each of the third set of prepared samples, as well as the third blank, from a 100mM stock, before each was scanned again using the settings outlined in section 3.2.5.2 but with the detector voltage set to 750V. Finally, 20mM SDS and 50μM ATP were added to the fourth set of UCP2 samples and the fourth blank, from 693mM and 100mM stocks, respectively and were scanned using the same settings as were used for the previous samples.

3.2.7 Detergent Mediated Reconstitution and Acrylamide Quenching of UCP2 Trp Fluorescence

3.2.7.1 Detergent Mediated Reconstitution of UCP2 for Quenching of Trp Fluorescence with Acrylamide

In order to study the UCP2 mutants in a more native-like environment, they were reconstituted into proteoliposomes, using detergent mediated reconstitution. First, 38μL of 100mg/mL of L-α-lecithin, in a chloroform methanol mix, was deposited into a 25mL round bottom flask, and dried under a stream of Ar gas. Any of the residual chloroform:methanol mixture was then evaporated by drying in a vacuum desiccator for 12h in the dark. After drying of the lipids was complete, the stock of the purified UCP2 mutant being reconstituted was obtained from the -80°C freezer and allowed to thaw completely on ice. The flask containing the dry lipids was then removed from the vacuum desiccator and the lipids were rehydrated with 240μL of D.B. The flask was then gently vortexed to remove all of the lipid from the sides of the flask. Next, 10μL of C_8E_4 detergent was added from stock, to give a detergent:lipid ratio of 2.5, by mass and the flask was gently vortexed to mix. The lipids in the flask were then allowed to fully resolubilise before 100μL of the mixture was removed and mixed with 1.9mL of the selected purified UCP2 mutant in D.B. at stock concentration, which varied by experiment and was corrected for by performing protein assays on all samples and standardizing with respect to micromolar protein concentration. The resulting mixture was incubated at 4°C for 30min with gentle stirring, yielding mixed micelles of detergent protein and lipid. Blank samples were also prepared in parallel with all protein samples by mixing

150µL of the lipid-detergent-buffer mixture with 2.85mL of D.B. and were also incubated at 4°C for 30min.

Proteoliposome formation was then induced by removal of the detergents using *SM-2 Biobeads* (Bio-Rad). Each 1mL of sample and Blank was added to a 1mL spin column of *SM-2 Biobeads* (Bio-Rad) and incubated on a rotator at 4°C for 2h. After the two hour incubation, the samples were removed from the column by 1min of centrifugation at 1000RPM for in a *Clinical 100* centrifuge (VWR). Every 1mL of sample or blank was then added to a second 1mL spin column of *SM-2 Biobeads* and incubated at 4°C on a rotator for 1h. The samples were again removed from the columns by centrifugation at 1000RPM for in a *Clinical 100* centrifuge (VWR) for 1min. The resulting samples and blanks were then used directly to run fluorescence quenching experiments with acrylamide, as described in the following section.

3.2.7.2 Quenching of Trp Fluorescence with Acrylamide for UCP2 Reconstituted in Proteoliposomes

The reconstituted UCP2 samples and blank liposomes produced in section 3.2.7.1 were used to run acrylamide quenching assays of UCP2 Trp Fluorescence with the aim of determining the accessibility of each of the two Trp residues present in UCP2. This was achieved by first loading 800µL of blank liposome into a quartz cuvette with a 1cm pathlength and scanning with 280nm and then 295nm excitation, using a *Cary® Eclipse* spectrofluorometer (Varian) with a scan rate of 600nm/min and the excitation slit width set to 2.5nm and detector voltage set to 800V. After the initial scan, 4µL of 9.447M acrylamide was added, the solution was

mixed in the cuvette by pipetting back and forth 3 times using a 10:100μL pipette (VWR) set to 50μL allowed to mix for 1min and then scanned again using the same conditions. Next, 19 more 4μL additions of 9.447M acrylamide were added with scans performed as described for the blank liposome, between each addition, thereby yielding 20 acrylamide data points for each sample, with the final concentration after each addition shown in table 5 and a final volume change of 10%.

The proteoliposome samples (800μL), containing the selected UCP2 Trp mutant or wt UCP2, were again scanned at 280nm and 295nm using the same conditions described for the blank. The same acrylamide additions and subsequent fluorescence scans were then made for the UCP2 samples, as described above, yielding 20 acrylamide data points for each sample, with the final concentration after each addition shown in table 5 and a final volume change of 10%. The resulting blank liposome spectra at each acrylamide point were subtracted from the corresponding UCP2 spectra at each acrylamide concentration, giving the baseline corrected spectra. A Bradford assay was then performed on each and the spectra for the UCP2 samples were then standardized by dividing by the micromolar concentration of protein, corrected for dilution after each acrylamide addition. The experiment was then repeated at pH 6.8 in the presence and absence of 100μM ATP. After all of the measurements were made and corrected for buffer effects and standardised with respect to micromolar concentration of protein in each sample, as well as the dilution after the given number of acrylamide additions, Stern-Volmer plots were generated by plotting the original fluorescence without acrylamide

divided by the fluorescence after a given number of acrylamide additions, against the molar concentration of acrylamide in the sample after those additions. The constants of dynamic quenching in each sample could then be derived from the slope of the linear trend line of each plot according to the relationship seen in equation 1. Where K_d is the constant of static quenching, [Q] is the concentration of quenching agent corresponding to a given peak fluorescence level F and F_0 is the peak fluorescence in the same sample prior to addition of any quenching agent [41].

$$\frac{F_0}{F} = k_D[Q] + 1 \text{ (Equation 1)}$$

Table 5: Acrylamide Concentration in Quenching Samples after a Given Number of Additions from a Stock: Concentration of acrylamide in fluorescence samples after a given number of 4µL additions from a 9.447M stock.

#of Acrylamide Additions	[Acrylanmide] (mM)
0	0
1	47
2	93
3	139
4	185
5	230
6	275
7	319
8	363
9	406
10	449
11	492
12	534
13	576
14	617
15	658
16	699
17	739
18	778
19	818
20	858

3.2.8 UCP2 Proton Transport Assay

3.2.8.1 Detergent Mediated Reconstitution of UCP2 for Proton Transport Assay

In order to study the UCP2 mutants in a more native-like environment, they were reconstituted into proteoliposomes, using detergent mediated reconstitution. First, 600µL of 100mg/mL of L-α-lecithin, in a chloroform methanol mix, was deposited into a 25mL round bottom flask, and dried under a stream of Ar gas. Any of the residual chloroform:methanol mixture was then evaporated by drying in a vacuum desiccator for 12h in the dark. After drying of the lipids was complete, the stock of the purified UCP2 mutant being reconstituted was obtained from the -80°C freezer and allowed to thaw completely on ice. The flask containing the dry lipids was then removed from the vacuum desiccator and the lipids were rehydrated with 1.35mL of 10mM SPQ in ultrapure water. The flask was then gently vortexed to remove all of the lipid from the sides of the flask. Next, 150µL of C_8E_4 detergent was added from stock, to give a detergent:lipid ratio of 2.5, by mass and the flask was gently vortexed to mix. The lipids in the flask were then allowed to fully resolubilise before 3mL of the selected purified UCP2 mutant, in 1.5x I.B., was deposited and the resulting mixture was incubated at 4°C for 1h with gentle stirring, yielding mixed micelles of detergent protein and lipid. Proteoliposome formation was then induced by removal of the detergents using *SM-2 Biobeads* (Bio-Rad). Each 1mL of sample and Blank was added to a 2mL spin column of *SM-2 Biobeads* (Bio-Rad) and incubated on a rotator at 4°C for 2h. After the two hour incubation, the samples

were removed from the column by 1min of centrifugation at 1000RPM for in a *Clinical 100* centrifuge (VWR). Every 1mL of sample or blank was then added to a second 2mL spin column of *SM-2 Biobeads* and incubated at 4°C on a rotator for 1h. The samples were again removed from the columns by centrifugation at 1000RPM for in a *Clinical 100* centrifuge (VWR) for 1min. External SPQ was then removed by gel filtration on a 3mL spin column of coarse grade *Sephadex-G25* (G.E. Healthcare) which was first equilibrated with I.B. Six such spin columns were produced for each proton transport experiment and 280µL of proteoliposome sample was added to each column before spinning at 2000RPM for 2min in a *JS13.1* swinging bucket rotor (Beckman-Coulter). The gel filtered proteoliposomes were then collected and used to run proton transport experiments, as described in the following section.

3.2.8.2 Proton Transport Assay for UCP2

To determine the proton flux rate, the kinetics of the change in SPQ fluorescence signal were measured with a *Cary® Eclipse* spectrofluorometer (Bio-Rad) with all measurements made in a quartz cuvette with a 1cm pathlength. SPQ fluorescence was excited at wavelength of 347nm and emission was monitored at 442nm, with both the excitation and emission slit widths set to 5nm. During the scans the temperature was held constant at 25^0C and the solution inside the cuvette was continuously stirred. Proton transport assay samples were prepared by mixing 40µL of proteoliposomes from section 3.2.8.1 with 1.96mL of 1X external buffer (Ex.B.) (80mM K_2SO_4, 40mM K-TES, 1mM EDTA, pH7.2) in the cuvette and then scanning. At 30s into each scan 5µL of 40µM sodium palmitate (PA) was added to the cuvette and an increase in fluorescence signal was observed. At 1min 2µL of

1mM valinomycin (val) was added to begin proton transport. The kinetics of proton transport was then measured for the next 4min for a total time of 5min/scan. Blank measurements were also obtained by running liposomes prepared as described in section 3.2.8.1 but with the 1.5XI.B. that was added containing no protein. A minimum of 6 scans were performed for each protein sample every time the assay was performed (figure 11) [28].

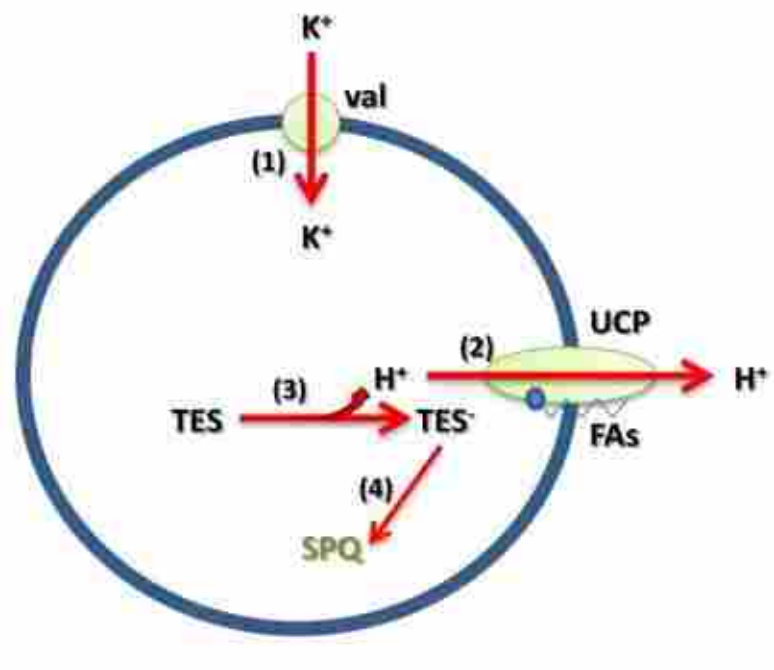

Figure 11: Schematic Representation of the Proton Transport Assay: Diagram showing a basic representation of the proton transport assay used in this project. In brief: (1) the addition of valinomycin to proteoliposomes containing UCP@ with TES buffer and SPQ fluorescent probe contained in the internal compartment and a K^+ gradient from the outside of the proteoliposomes to the inside, results in the influx of K^+ into the proteolipsomes. Prior to this addition the charge is balanced on both sides of the model membrane and so the addition of valinomcyin results in a buildup of positive charge on the inside of the proteoliposomes. This excess positive charge in the internal compartment of the proteoliposomes then provides the driving force for FFA activated, UCP2-mediated transport of protons out of the proteoliposomes (2), thereby reducing the charge gradient. This efflux of protons results in the deprotonation of the TES buffer (3) to TES^-, which subsequently quenches the fluorescence of SPQ (4)[28].

After the proton transport measurements were taken, the SPQ fluorescence signal was then calibrated by mixing 40µL of proteoliposome sample with 1.96mL of 1XI.B. and mixed for 20 seconds before scanning using the same conditions used for measuring proton transport. At 20s in each scan 2µL of 1mM nigericin (K^+/H^+ ionophore) was added to the cuvette and a decrease in fluorescence was observed. At 45s and at every 15th second afterward until seven additions had been made, 2µL of 2M KOH was added to the cuvette. The calibration fluorescence was then fitted to the modified Stern-Volmer equation, equation 2.

$$\frac{F_0}{F} = k_q[H^+] + 1 \quad \text{(Equation 2)}$$

Where F_0 is the fluorescence signal immediately prior to the first addition of KOH, F is the fluorescence signal after addition of KOH, k_q is the Stern-Volmer constant and $[H^+]$ is the change of proton concentration in the media [28, 56]. The fitted calibration data was then used to determine k_q which was subsequently utilized to convert fluorescence kinetic data into proton efflux using equation 3.

$$[H^+] = \frac{F_0 - F}{F} \times \frac{1}{k_q} \quad \text{(Equation 3)}$$

Next, the total internal volume of the proteoliposomes was determined for each set of scans. This was done by first mixing 40µL of proteoliposomes sample with 1.96mL of ultrapure water, mixing for 20s and then scanning using the same conditions outlined for measurement of proton transport. At 20s in each of the internal volume determination runs, 5µL of 0.25% (w/v) C_8E_4 was added to disrupt

the proteoliposomes and an increase in fluorescence was observed. At 45s and at every 15th second afterward, until seven additions had been made, 2.5µL of 100µM SPQ was added. The SPQ fluorescence signal was then plotted against the $[SPQ]_{added}$ to obtain the original concentration of SPQ in the proteoliposomes ($[SPQ]_{proteoliposomes}$). The $[SPQ]_{proteoliposome}$ was then compared to the original concentration of SPQ added to the sample ($[SPQ]_0$=3mM) in order to determine the internal volume of the proteoliposomes via the relationship detailed in equation 4 [28, 56].

$$V(\mu L) = \frac{[SPQ]_{proteoliposome}}{[SPQ]_0} \text{ (Equation 4)}$$

The initial rate of proton transport was then determined from the plot of proton efflux versus time to obtain the maximum transport rate v_{max} (mM/s). v_{max} was next converted to v'_{max} (nmol/s) using equation 5.

$$v'_{max}(nmol/s) = v_{max}(mM/s) \times V(\mu L) \text{ (Equation 5)}$$

The rate of nonspecific proton leakage was determined by calculating the v'_{max} of the protein-free blank liposome scans and was subsequently subtracted from the rate of proton transport for the proteoliposome samples. The transport rates were finally normalised with respect to protein concentration, which was determined as described in section 3.2.8.3. Final proton transport rates were reported in units of µmol $H^+ \cdot min^{-1} \cdot$mg protein^{-1} [28, 56].

3.2.8.3 Determining Protein Concentration by TCA Precipitation and Modified Lowry Assay

To determine the protein concentration in the proton transport samples, 50µL, 80µL and 100µL aliquots of each as well as BSA standards were diluted to 1mL with ultrapure water were prepared in duplicate and then precipitated with 100µL of 0.15% (w/v) sodium deoxycholate (DOC) and 100µL of pure HPLC grade trichloroacetic acid (TCA). The precipitates were pelleted in a microcentrifuge by spinning at 15000RPM and 4^0C for 10min and the pellets were then redissolved in 25µL of 20% (w/v) SDS. 100µL of reagent A' from the *Bio-Rad RC DC Protein Assay* kit (Bio-Rad) was then added to each of the samples and standards, followed by bath sonication at room temperature for 5min and then 2min with no sonication before being bath sonicated again for 3min. 800µL of reagent B was then added to each of the samples and standards and they were incubated at room temperature for 30min before 300µL aliquots of each were added to a 96 well microplate and absorbance at 750nm was measured in a microplate reader (Varian).

4 RESULTS

4.1 Site-Directed Mutagenesis of UCP2 and Establishment of a Membrane-Targeted Recombinant Expression System in BL21 Codon Plus

The first goal of the project was to remove the endogenous NcoI restriction site present in the cDNA of UCP2 by incorporating a silent mutation, so that an NcoI restriction site could be incorporated on the 5' end to facilitate cloning into pET26b(+). This was accomplished using the site-directed mutagenesis technique known as primer-overlap extension PCR. In lane 4 of figure 12 a ~1kb band is seen, as was expected for a successful amplification and mutagenesis of *UCP2* which meant that the project could proceed to the cloning of the His-tagged *wt UCP2* into the pET26b(+) vector (henceforth referred to as *wt UCP2-pET26b(+)*. The pET26b(+) expression vector was chosen because it contains a pelB leader sequence which drives the targeting of attached proteins to the periplasm in gram negative bacteria. For an integral membrane protein such as UCP2, which by nature have a relatively high degree of hydrophobicity, the energy barrier for excretion through the membrane should be sufficiently high that the protein will not be able to pass through and will instead be embedded into the membrane [57].

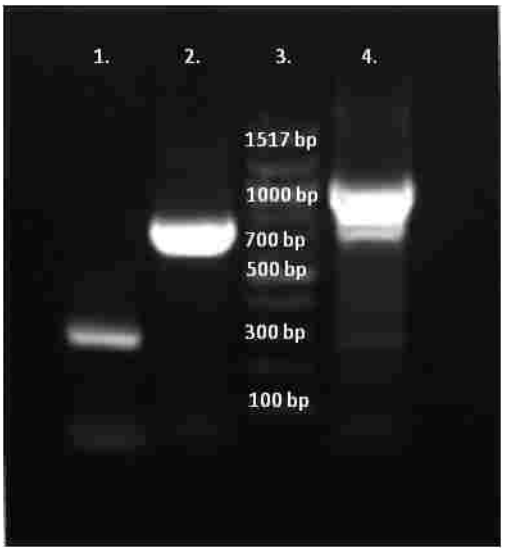

Figure 12: Agarose Gel Depicting the Results of NcoI Silencing in wt UCP2: An agarose gel showing the products of rounds one (lane 1), two (lane 2), and three (lane 4) of the site-directed mutagenesis of UCP2 by primer overlap-extension PCR used to produce the His-tagged UCP2 construct cloned into pET26b(+).

The newly produced His-tagged *wt UCP2* NcoI knockout was gel purified and subsequently restriction digested with NcoI-HF and HindIII-HF in parallel with isolated empty pET26b(+). The digestion products were then gel purified and allowed to ligate overnight after which the product of the ligation reaction was used to transform DH5α *E.coli* cells and colonies were selected. The presence of the *wt UCP2-pET26b(+)* construct was confirmed by colony PCR (figure 13) and plasmid was isolated from colonies confirmed, by colony PCR, to contain the *wt UCP2-pET26b(+)* construct used to isolate plasmid, which was then sent to TCAG for DNA sequencing (see appendix 2 for complete sequencing results). Based on the DNA sequencing results a colony confirmed to contain the correctly produced and oriented His-tagged *wt UCP2* in the pET26b(+) vector was selected and again grown up overnight and then used to make a glycerol stock.

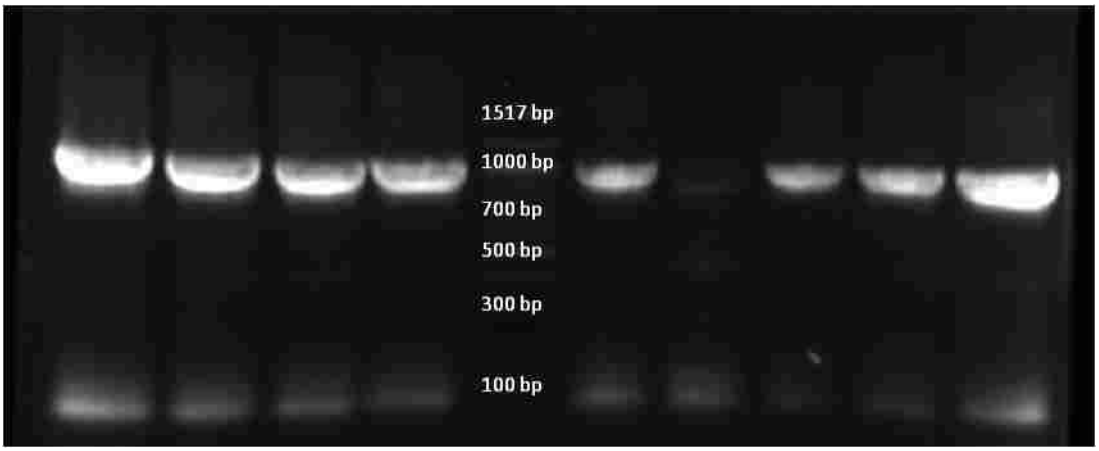

Figure 13: Agarose Gel Depicting the Results of Colony PCR for Transformation of *E.coli* with wt UCP2-pET26b(+): 0.8% agarose gel with ethidium bromide incorporated and run at 120V for 1h before imaging on a *VersaDoc 4000 Gel Imaging System* (Bio-Rad) with a 100bp ladder. The gel shows the results of colony PCR on DH5α *E.coli* cells following their transformation with His-tagged *wt UCP2*-pET26b(+). The presence of bands at ~1kb is indicative of the presence of the His-tagged *wt UCP2* insert in the selected colony.

The glycerol stock of the *wt UCP2-pET26b(+)* in DH5α was then used to inoculate an overnight culture which was then used to isolate *wt UCP2-pET26b(+)* plasmid. The isolated plasmid was then used as the template for the site-directed mutagenesis reactions used to produce the two single Trp mutants of UCP2 (W176Y and W283F). Tyr and Phe were chosen as substitutes for the W176 and W283 residues, respectively, to minimise the impact of the mutations on the conformation of UCP2 based on the fact that they are the other two proteogenic aromatic amino acids and should be the most similar to Trp. The reason Tyr was chosen as the substitute for the W176 residue whereas Phe was chosen for the W283 residue, was because Tyr residues are more polar than Phe residues and predictions of the topology of UCP2 in membranes, based on hydropathy plots (figure 3A), place the W176 residue near the membrane interface and the W283 residue more towards

the middle of the membrane, in the hydrophobic tail region. The success of the PCR reactions was again confirmed by gel electrophoresis on a 0.8% agarose gel, as described above for His-tagged *wt UCP2* with the endogenous NcoI restriction site knocked out. The single mutants were then, digested, cloned into pET26b(+) and transformed into DH5α *E.coli* cells as described previously for *wt UCP2-pET26b(+)*. The success of the transformation reactions were then evaluated by colony PCR as described previously (figure 14) and the colonies confirmed to contain the plasmid and insert were used to grow overnight cultures before plasmid was isolated and sent to TCAG for sequencing (see appendix 2 for full sequencing results). A colony that was confirmed by sequencing to contain the full length UCP2 coding sequence with the desired mutation incorporated (TGG→TAC and TGG→TTC for W176Y and W283F, respectively) was selected for each mutant, then grown overnight and used to prepare a glycerol stock.

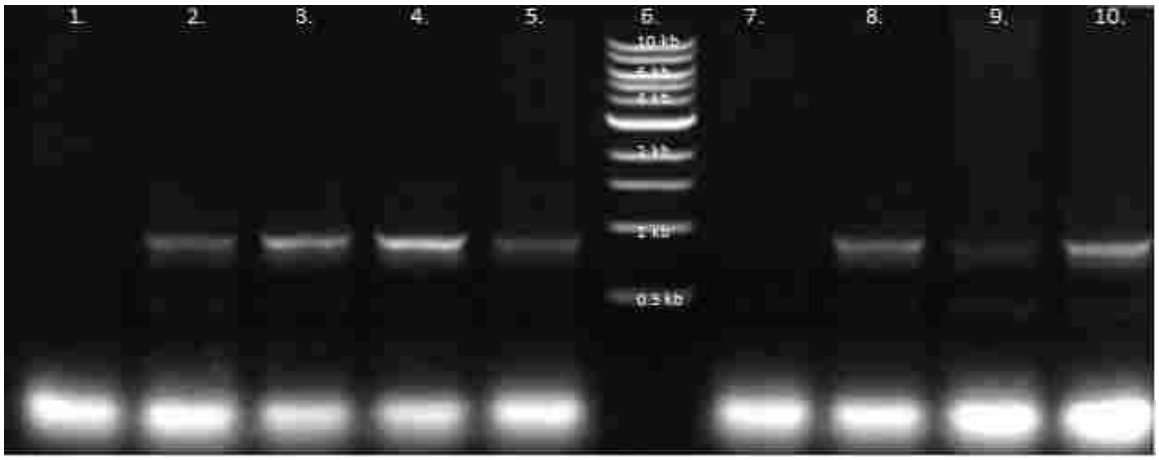

Figure 14: Agarose Gel Depicting the Results of Colony PCR for Transformation of *E.coli* with W176Y and W283F UCP2-pET26b(+): 0.8% agarose gel with ethidium bromide incorporated and run at 120V for 1h before imaging on a *VersaDoc 4000 Gel Imaging System* (Bio-Rad) with a 1 kb ladder. The gel shows the results of colony PCR on DH5α *E.coli* cells following their transformation with His-tagged *W176Y UCP2*-pET26b(+) (lanes 1-5) and His-tagged *W283F UCP2*-pET26b(+) (lane 7-10). The presence of bands at

~1kb is indicative of the presence of the His-tagged *UCP2* Trp mutant insert in the selected colony.

The glycerol stock of the *W176Y UCP2-pET26b(+)* in DH5α was then used to inoculate an overnight culture which was then used to isolate *W176Y UCP2-pET26b(+)* plasmid. The isolated plasmid was then used as the template for the site-directed mutagenesis reactions used to produce the double Trp mutant of UCP2 (W176Y-W283F). The success of the PCR reactions was again confirmed by gel electrophoresis on a 0.8% agarose gel, as described above for His-tagged *wt UCP2* with the endogenous NcoI restriction site knocked out (figure 15). The W176Y-W283F mutant was then, digested, cloned into pET26b(+) and transformed into DH5α *E.coli* cells as described previously for *wt UCP2-pET26b(+)*. The success of the transformation reactions were then evaluated by colony PCR as described previously and the colonies confirmed to contain the plasmid and insert were used to grow overnight cultures before plasmid was isolated and sent to TCAG for sequencing (figure 16, see appendix 2 for full sequencing results). A colony that was confirmed by sequencing to contain the full length UCP2 coding sequence with the desired mutation incorporated (TGG→TAC and TGG→TTC for W176Y and W283F, respectively) was selected for each mutant, then grown overnight and used to prepare a glycerol stock.

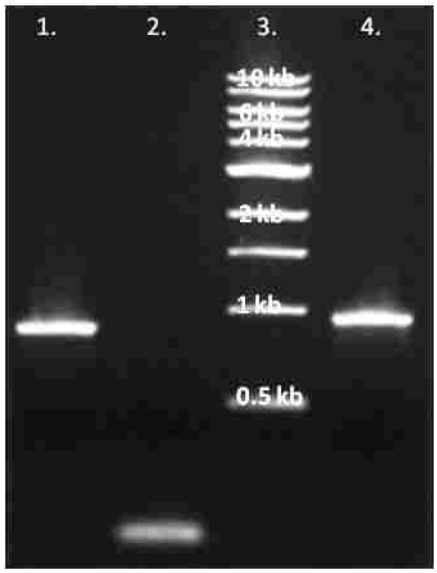

Figure 15: Agarose Gel Depicting the Results of Site-Directed Mutagenesis of W176Y UCP2 to W176Y-W283F: 0.8% agarose gel with ethidium bromide incorporated and run at 120V for 1h before imaging on a *VersaDoc 4000 Gel Imaging System* (Bio-Rad). The gel shows the products of rounds one (lane 1), two (lane 2), and three (lane 4) of the site-directed mutagenesis of UCP2 by primer overlap-extension PCR used to produce the His-tagged W176Y-W283F UCP2 mutant.

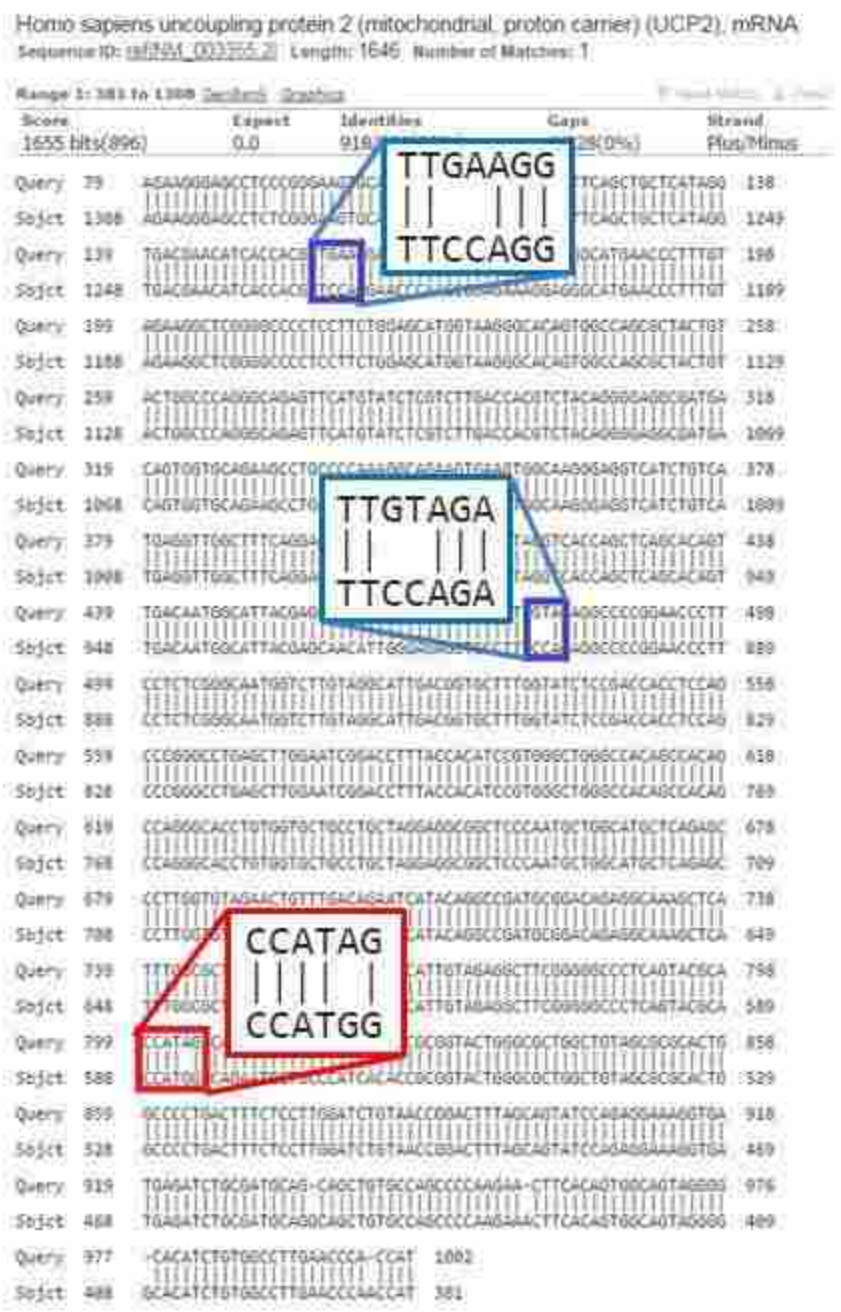

Figure 16: Result for T7 Terminator Primed DNA Sequencing of W176Y-W283F UCP2-pET26b(+): The results of DNA sequencing of the *W176Y-W283F UCP2-pET26b(+)* plasmid with a T7 terminator primer (Query line) aligned with the wt UCP2 mRNA sequence using the nucleotide Basic Local Alignment Search Tool (nBLAST) available from NCBI [58]. The top and bottom blue boxes show the nucleotide changes resulting in the W283F and W176Y mutations, respectively. The red box shows the silent mutation introduced to knockout the endogenous NcoI restriction site.

Once it was confirmed by DNA sequencing that all of the required *UCP2-pET26b(+)* constructs had been produced and successfully transformed into DH5α, a plasmid isolation was performed for each of them and the isolated plasmid was then used to transform BL21 CD^+. Plasmid was again isolated for each of the UCP2 constructs, this time from BL21 CD^+ and sent to TCAG for DNA sequencing and it was confirmed that each of the UCP2-pET26b(+) constructs was successfully transformed into BL21 free of any undesired mutations (figure 16, see appendix 2 for full sequencing results).

4.2 Membrane-Targeted Expression of hUCP2 Mutants in BL21 Codon Plus and Purification by IMAC

After it was confirmed by DNA sequencing that all of the UCP2-pET26b(+) constructs that were required for the project had been produced and successfully cloned into BL21 CD^+ the next step was to overexpress each of the UCP2 mutants, and the wt by autoinduction using the method that had been established for UCP1 by prior work done in our lab and outlined in detail above in section 3.2.7 [57]. The cells were then lysed as previously described and the success of the expression of wt UCP2 and the selective Trp mutants as well as its targeting to the bacterial membrane were confirmed by: isolating the bacterial membranes via differential centrifugation; purifying the UCP from the bacterial membrane via IMAC; and finally detecting the presence of UCP2 in the purified samples by western blot (see figures 17 and 18).

Figure 17 shows single bands in each lane of a western blot with an anti-6X his antibody, corresponding to the typical apparent M_w of UCP2 monomer bands on an SDS-PAGE gel, which is ~25kDa [40]. The lanes in the western blot were loaded with wt UCP2, W176Y, W283F and W176Y-W283F therefore confirming the confirming their expression into the bacterial membrane and successful isolation by differential centrifugation and IMAC. In order to definitively confirm UCP2 as the source of the bands seen in the anti-his western blot a second western blot was run with an anti-UCP1 antibody with established cross-reactivity with UCP2 [59]. Figure 18 shows the results of the anti-UCP1 western blot with bands again apparent at ~25kDa which is the expected M_w for the UCP2 monomer. Interestingly bands at ~50kDa and ~100 kDa were detected in the anti-UCP1 western blot, potentially corresponding to dimer and tetrameric bands, as previously reported for UCP1 [57]. The SDS-PAGE gel shown in figure 19 was run with purified stocks of wt UCP2 and each of the selective Trp mutants. The presence of multiple bands in each lane of the SDS-PAGE gel, especially the bands corresponding to M_w values higher than that of UCP2 (apparent M_w ~30kDa), is problematic and may explain the fluorescence results obtained, as discussed below in chapter 5. Nevertheless, due to the presence of higher molecular weight bands in the anti-UCP1 western blot and previous work showing the effectiveness of the same purification system for UCP1, these bands were potentially misattributed to oligomerization of UCP2 and the project moved forward to fluorescence assays [57].

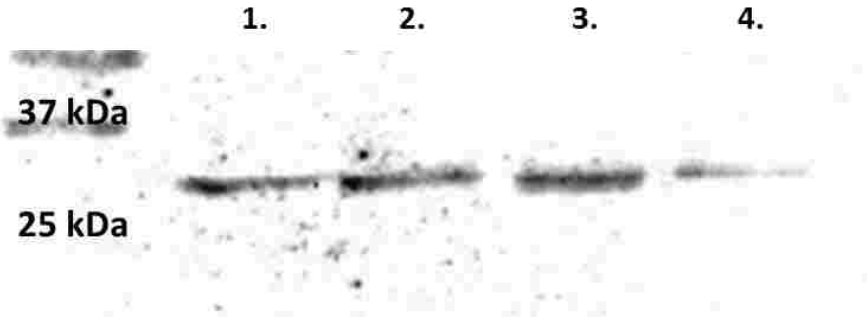

Figure 17: Western Blot of Purified Stocks of wt UCP2 and Selective Trp Mutants – Anti-His: Chemiluminescent western blot detection of his-tagged wt UCP2 and the selective Trp mutants of UCP2 using anti-his primary antibody from a mouse host and an anti-mouse/HRP conjugated secondary antibody from a rabbit host. The bands present between 37kDa and 25kDa are indicative of the presence of his-tagged recombinant UCP2. Lanes 1-4 were loaded with purified samples of wt UCP2, W176Y UCP2, W283F UCP2 and W176Y-W283F UCP2, respectively.

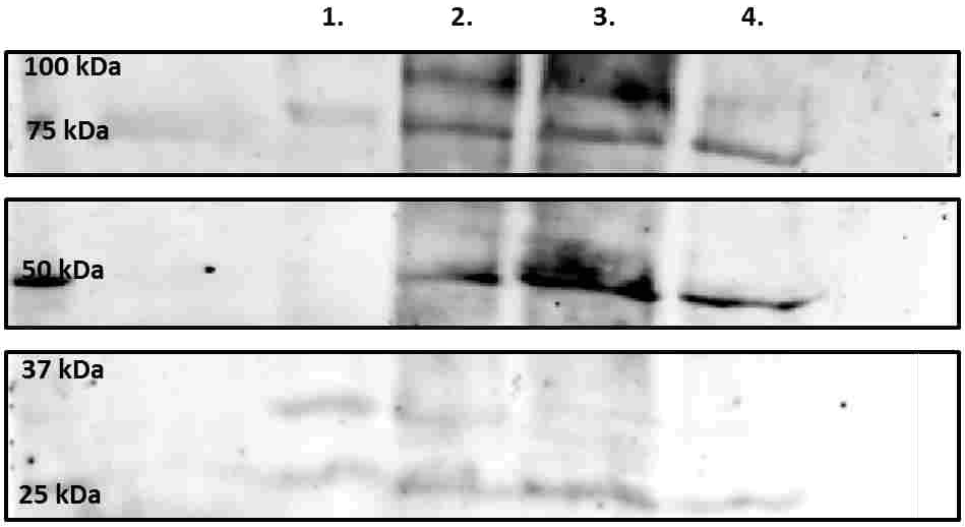

Figure 18: Western Blot of Purified Stocks of wt UCP2 and Selective Trp Mutants – Anti-UCP1: Chemiluminescent western blot detection of his-tagged wt UCP2 and the selective Trp mutants of UCP2 using anti-UCP1 primary antibody from a rabbit host and an anti-rabbit/HRP conjugated secondary antibody from a goat host. The bands present between 37kDa and 25kDa are indicative of the presence of his-tagged recombinant UCP2. Lanes 1-4 were loaded with purified samples of wt UCP2, W176Y UCP2, W283F UCP2 and W176Y-W283F UCP2, respectively.

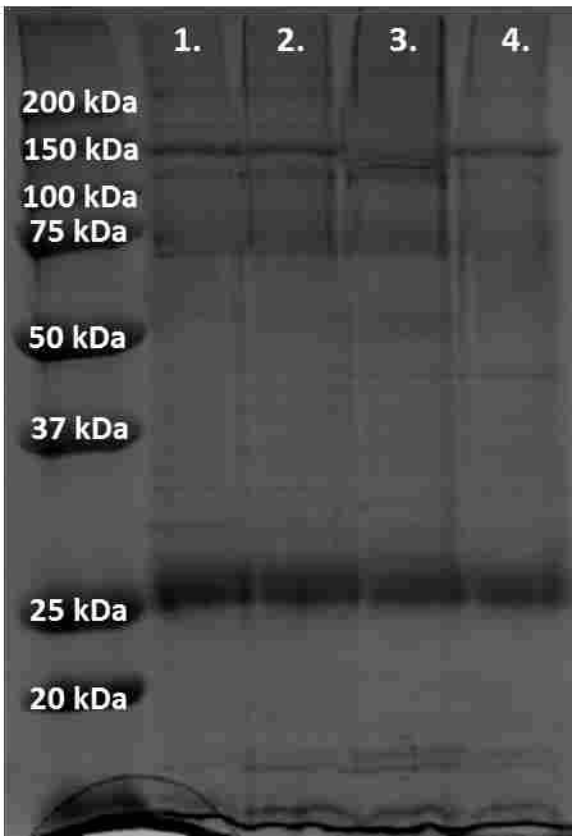

Figure 19: SDS-PAGE Gel Run with Purified Stocks of wt UCP2 and Selective Trp Mutants: SDS-PAGE gel, stained with Coomassie Blue, showing the results of the purification of UCP2 wt and Trp mutants from BL21 by differential centrifugation, IMAC and desalting. Lanes 1-4 were loaded with the purified stock of wt UCP2, W176Y, W283F and W176Y-W283F, respectively.

4.3 Confirmation of the Conformation Equivalence of the Selective Trp Mutant of UCP2 by Far-UV CD Spectroscopy

Once the successful production, membrane targeting and purification of the selective Trp mutants of UCP2, as well as wt UCP2, had been confirmed by SDS-PAGE and western blot the next goal was to confirm that the selective Trp mutants retained conformational equivalence to wt UCP2. This was done by far-UV CD spectroscopy scans overlaying them as described in section 3.2.5 (figure 20). As can be seen in figure 20, the Trp mutants retained dominantly helical conformations as evidence by the local minima

at 208nm and 222nm. It can also be seen that the selective Trp mutants retain conformational equivalence with the wt protein as evidenced by the overlapping of the W176Y-W283F mutant's far-UV CD spectrum with that of the wt. Despite a slight gap between the spectra, the W176Y and W283F mutants were also confirmed to retain conformational equivalence with the wt protein based on the overall secondary structure composition of the proteins, with the difference seen in the absolute molar elipticity accounted for by the error range in the protein assay used to determine the [UCP2] in each sample.

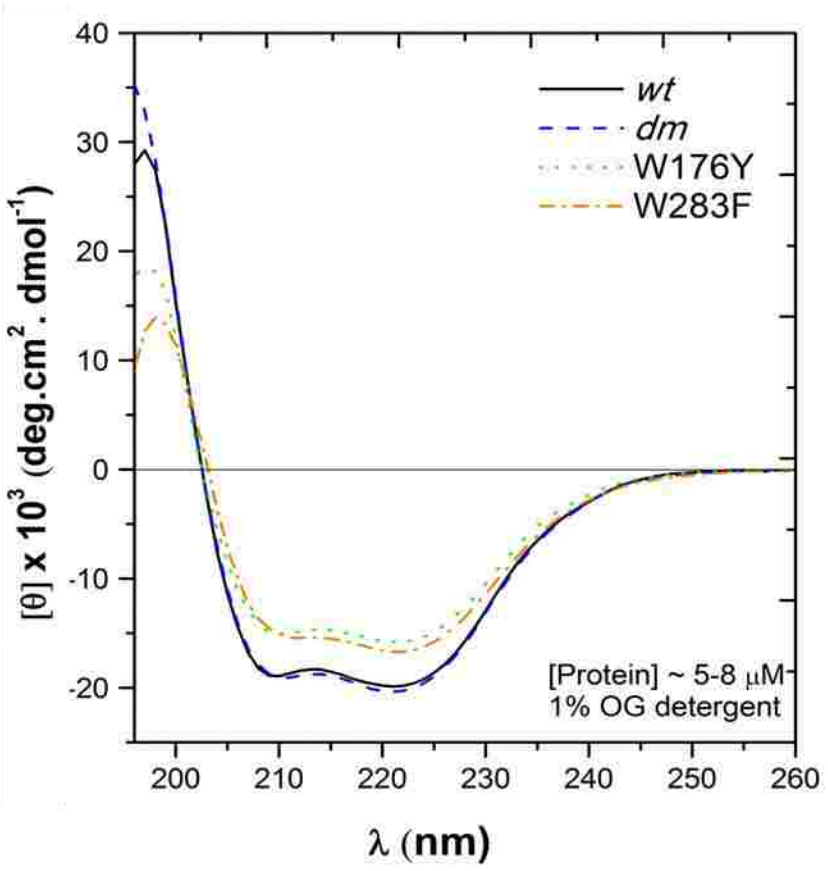

Figure 20: Far-UV CD Spectra of Selective Trp mutants of UCP2: Far-UV CD spectra of selective Trp mutants of UCP2 and wt UCP2 in a detergent system consisting of 1% OG.

4.4 Intrinsic Fluorescence Based Assays for Selective Trp Mutants of UCP2

4.4.1 Intrinsic Fluorescence Measurement in Detergent

The fluorescence of the purified selective Trp mutants of UCP2 was assessed and compared against the wt fluorescence. For each sample both the total intrinsic fluorescence (excitation at 280nm) and the tryptophan specific fluorescence (excitation at 295nm) was measured (figure 21). The intrinsic fluorescence based assays did not show the expected low intrinsic fluorescence for the double mutant when excited at 295nm. Furthermore, it was expected that there would be a stepwise decrease in the fluorescence of the proteins samples with wt UCP2 having the highest fluorescence, followed by each of the single Trp mutants (W176Y and W283F) and finally the W176Y-W283F double Trp mutant having the lowest. However, this was not the case, as can be seen in Trp fluorescence spectra shown in figure 21B, which shows the peak of the wt UCP2 roughly overlapping with the W283F mutant and the peak of the W176Y mutant roughly overlapping with that of the W176Y-W283F double mutant. The overlap between the wt UCP2 and W283F and between W176Y and W176Y-W283F suggests that the fluorescence of the W283 residue may be fully quenched in the wt protein.

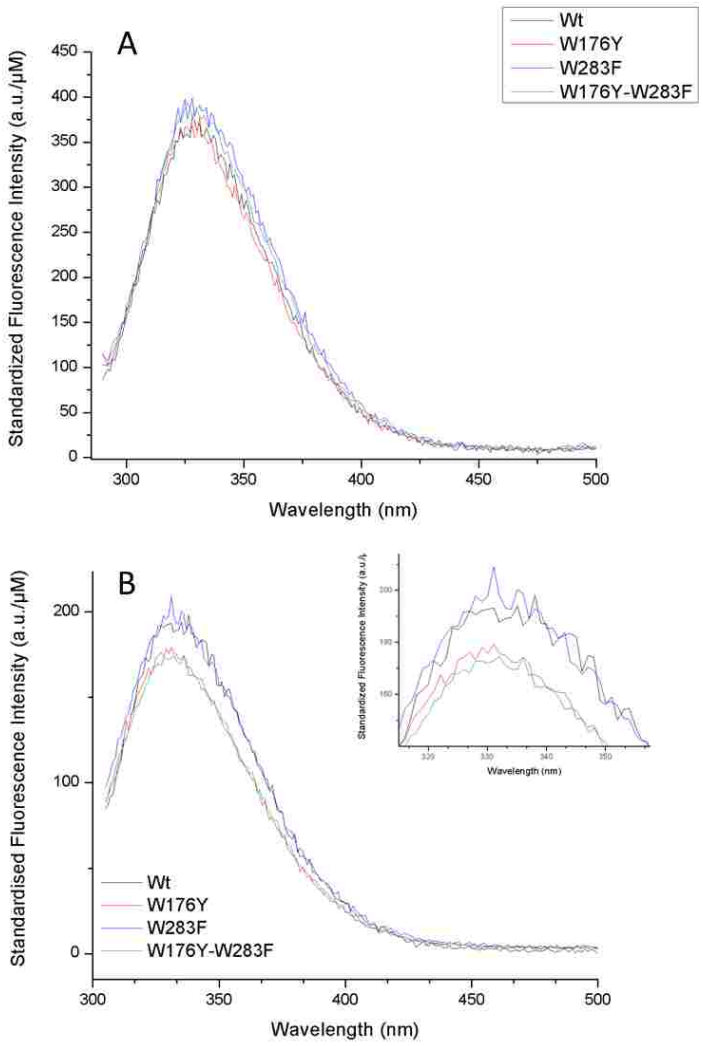

Figure 21: Intrinsic Fluorescence Spectra of Selective Trp mutants of UCP2: Fluorescence of purified samples of selective Trp mutants of UCP2 as well as the wt, in D.B. with excitation at 280nm (A) and 295nm (B) standardized with respect to micromolar concentration of protein in each sample.

Due to the unexpectedly high baseline fluorescence observed for the W176Y-W283F UCP2 mutant in the Trp emission spectrum more scans were run under varying buffer and scan conditions in order to determine the source of the aberration with the aim of mitigating it. The additional scans however, all showed the same high Trp fluorescence signal for the W176Y-W283F UCP2 mutant. Aside

from the high background fluorescence for the double knockout mutant the Trp fluorescence spectra shown in figure 21B still demonstrated a clear difference between the Trp fluorescence of the W176Y and W283F mutants, with higher peak fluorescence for the W283F mutant that was slightly red-shifted relative to the W176Y mutant.

4.4.2 SDS Denaturation Assay

In order to potentially help distinguish between the Trp fluorescence of the W176Y single mutant and the W176Y-W283F double mutant and also to investigate the position of the nucleotide binding site within the folded structure of UCP2 an SDS denaturation assay was devised in which the UCPs being examined were scanned to obtain baseline fluorescence measurements and then denatured by the addition of 20mM SDS in the presence and absence of 50μM ATP. It was expected that if the previously observed overlap between the fluorescence peaks of the wt UCP2 and W283F and between W176Y and W176Y-W283F were due to the quenching of W283 by some amino acid in close proximity or some other effect of protein folding, then upon SDS denaturation the expected stepwise decrease in the Trp fluorescence of the proteins, detailed in the previous section, would be observed. It was also expected that due to the predicted presence of the nucleotide binding site of UCP2 in close proximity to the W283 Trp residue there would be a lower increase in the peak Trp fluorescence of W176Y with 50μM ATP upon denaturation with 20mM SDS relative to W176Y with no ATP added due to the expected increase in stability of the local environment around W283 that would accompany ATP binding. By extension, the aforementioned effect of ATP addition

prior to denaturation with SDS for the W176Y should also be present for wt UCP2, should be decreased or absent for the W283F mutant and should be entirely absent for the W176Y-W283F double mutant.

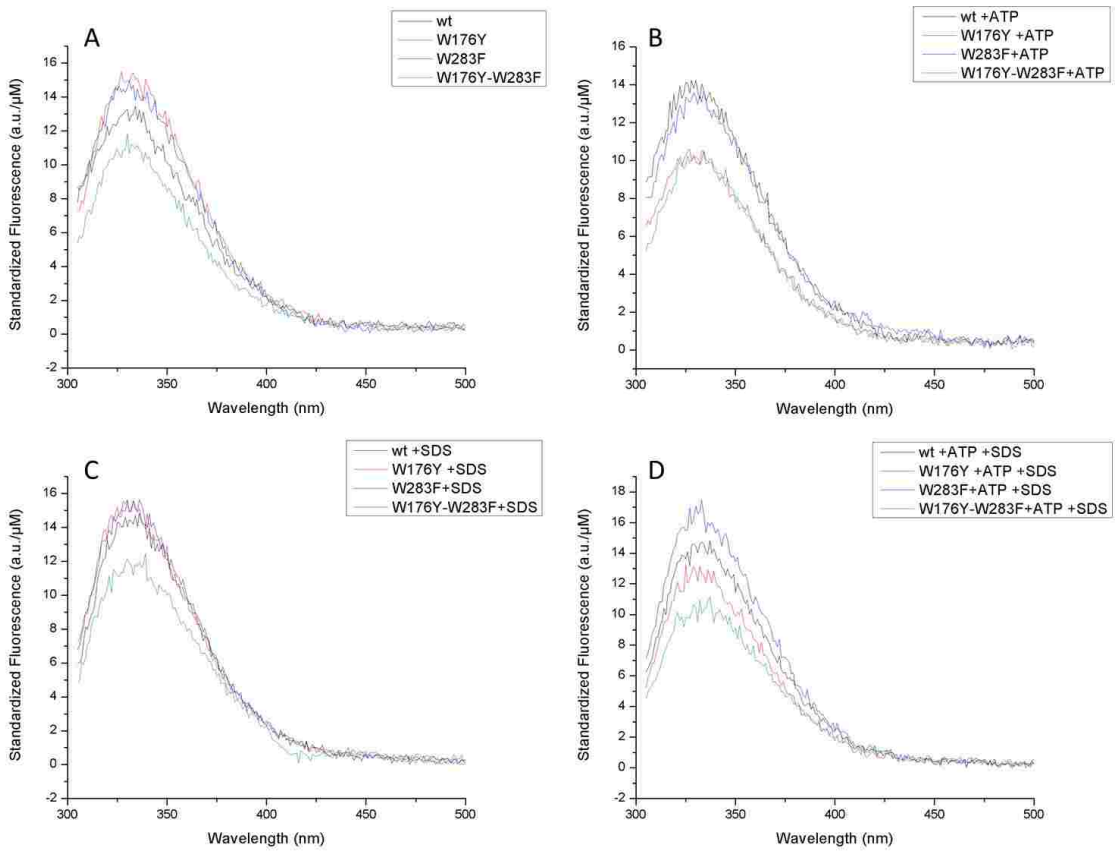

Figure 22: Fluorescence Spectra from SDS Denaturation Assay (All Conditions): Results of SDS denaturation assay showing scans of purified samples of selective Trp mutants of UCP2 as well as the wt, in D.B. with nothing added (A), 20mM SDS added (B), 50μM ATP (C) and both 50μM ATP and 20mM SDS (D). Excitation was at 295nm, and the spectra were standardized with respect to micromolar concentration of protein in each sample.

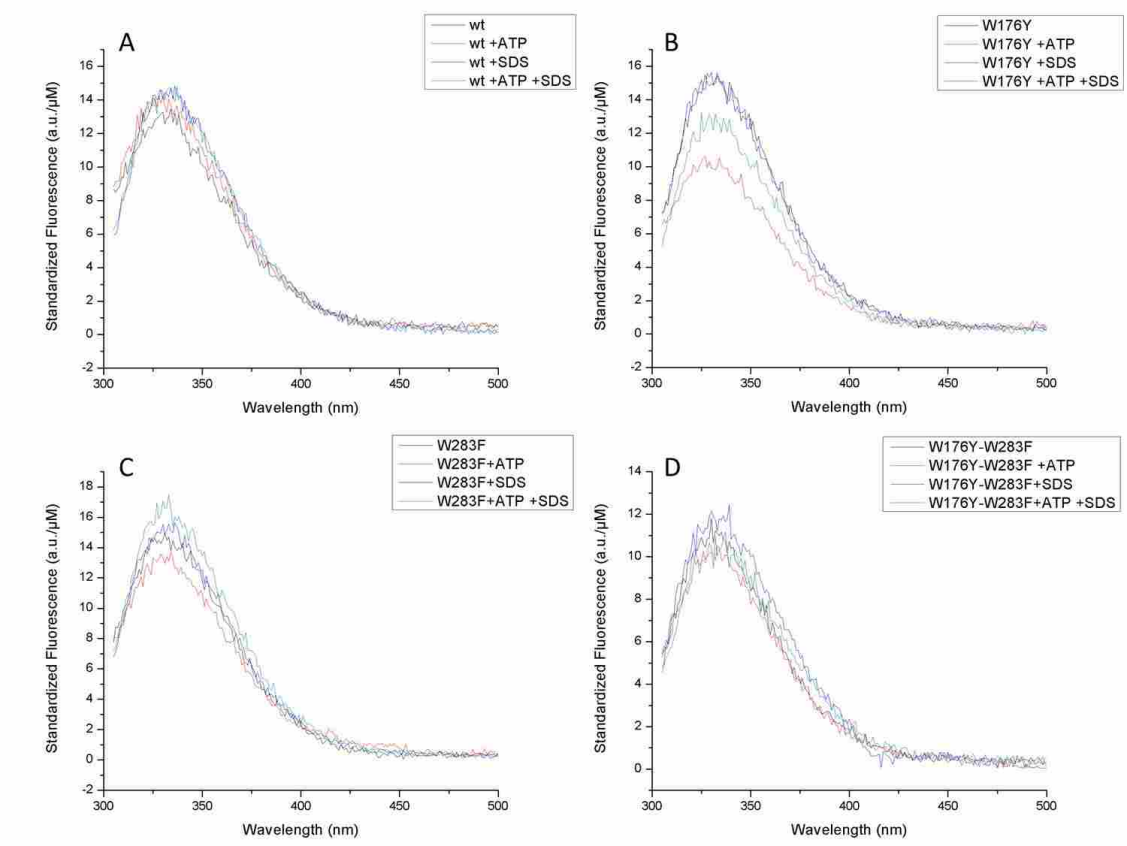

Figure 23: Fluorescence Spectra from SDS Denaturation Assay (All Mutants): Results of SDS denaturation assay showing scans of purified samples of wt (A), W176Y (B), W283F (C) and W176Y-W283F (D) UCP2, in D.B. with 50μM ATP added, 20mM SDS added, and both 50μM ATP and 20mM SDS added. Excitation was at 295nm, and the spectra were standardized with respect to micromolar concentration of protein in the samples.

Figures 22 and 23 show the results of the SDS denaturation assay of the selective Trp Mutants of UCP2 and wt UCP2. Figure 22A shows the results of the denaturation of wt UCP2 and the selective Trp mutants and demonstrates that denaturation did not restore the expected stepwise decrease in fluorescence between UCP2 wt, the single Trp mutants (W176Y and W283F) and the W176Y-W283F double mutant. Figure 23A displays the results of the SDS denaturation assay for the W176Y mutant and shows that W283 has maximum fluorescence in the folded UCP2 as evidenced by the lack of a significant increase in fluorescence signal upon denaturation with SDS, indicating it may be fully exposed to solvent in the folded UCP2. Figure 23A shows a clear decrease upon binding of ATP, which is not fully mitigated by denaturation with SDS. There is also a slight blue-shift in the peak emission wavelength of the W176Y mutant upon the addition of ATP. The results for the SDS denaturation assay performed on the W283F are displayed in figure 23B and shows that the fluorescence of the W176 residue was not increased by the addition of SDS alone suggesting either full exposure of the W176 residue to begin with or a highly stable local environment around W176. Figure 23B also shows a decrease in W176 fluorescence upon the addition of 50μM ATP, although the decrease is markedly smaller than the one observed for W283. This suggests that W176 is also close to the site of ATP binding in UCP2 but that W283 is closer or alternatively, that changes in the conformation of UCP2 upon binding of ATP, result in partial quenching of W176. Interestingly, the W283F fluorescence spectrum also shows that the addition of both ATP and SDS results in an increase in the

fluorescence signal of W176, implying that binding of ATP by UCP2 may lead to decreased stability around the W176 residue. Finally, while still retaining an unexpectedly high fluorescence signal overall, the spectra for the W176Y-W283F, seen in figure 23C double Trp mutant, containing no Trp residues was not sensitive to the addition of 20mM SDS, 50μM ATP or both 50μM ATP and 20mM SDS, which was the expected result.

4.5 Acrylamide Quenching of Selective Trp Mutant of UCP2 Reconstituted into Liposomes

The next step in this project was to the run fluorescence quenching assays with acrylamide on the selective Trp mutants of UCP2, as well as the wt protein, after reconstitution into model liposomes of L-α-Lecithin using a slight modification of the previously established detergent mediated reconstitution method for the UCPs [28]. The aim of this portion of the study was to distinguish between the accessibility of the two Trp residues present in UCP2 to the acrylamide quencher, while embedded in a model membrane and thereby provide insight into the overall membrane topology of UCP2. Additionally, acrylamide quenching experiments were performed at pH 6.8 in the presence and absence of 100μM ATP in order to provide further insight into the position of the nucleotide site in UCP2. The results of the acrylamide quenching experiments are shown in figures 24-27 and table 6.

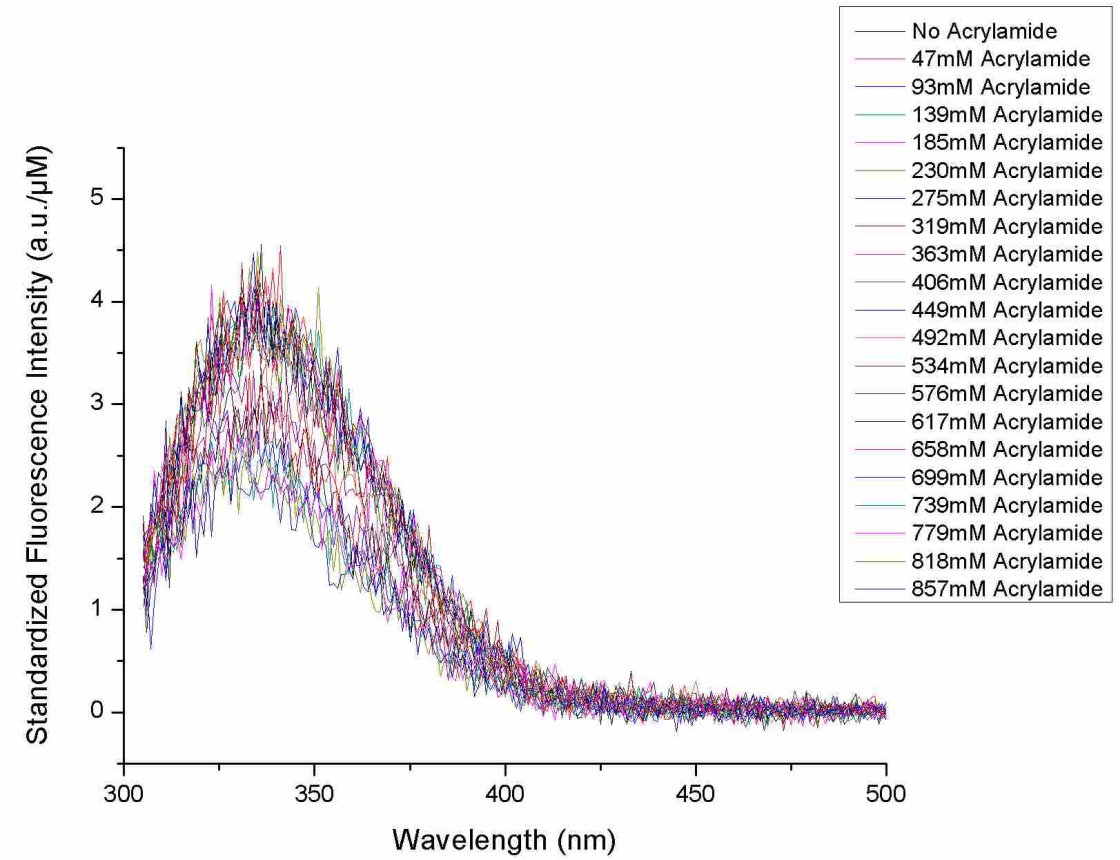

Figure 24: Acrylamide Quenching Spectra of *wt* UCP2 : Spectra obtained from fluorescence quenching with acrylamide for wt UCP2 at pH 8.0 and excitation at 295nm.

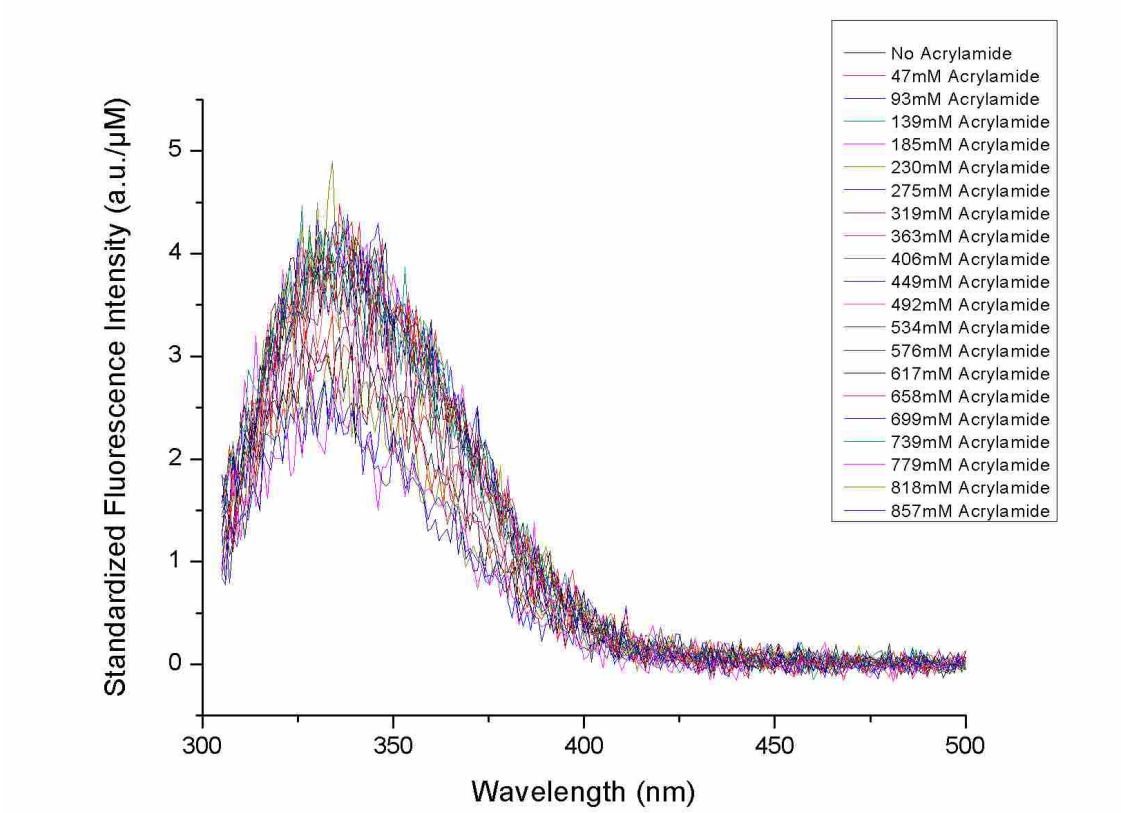

Figure 25: **Acrylamide Quenching Spectra of W176Y-W283F UCP2:** Spectra obtained from fluorescence quenching with acrylamide for W176Y-W283F UCP2 at pH 8.0 and excitation at 295nm.

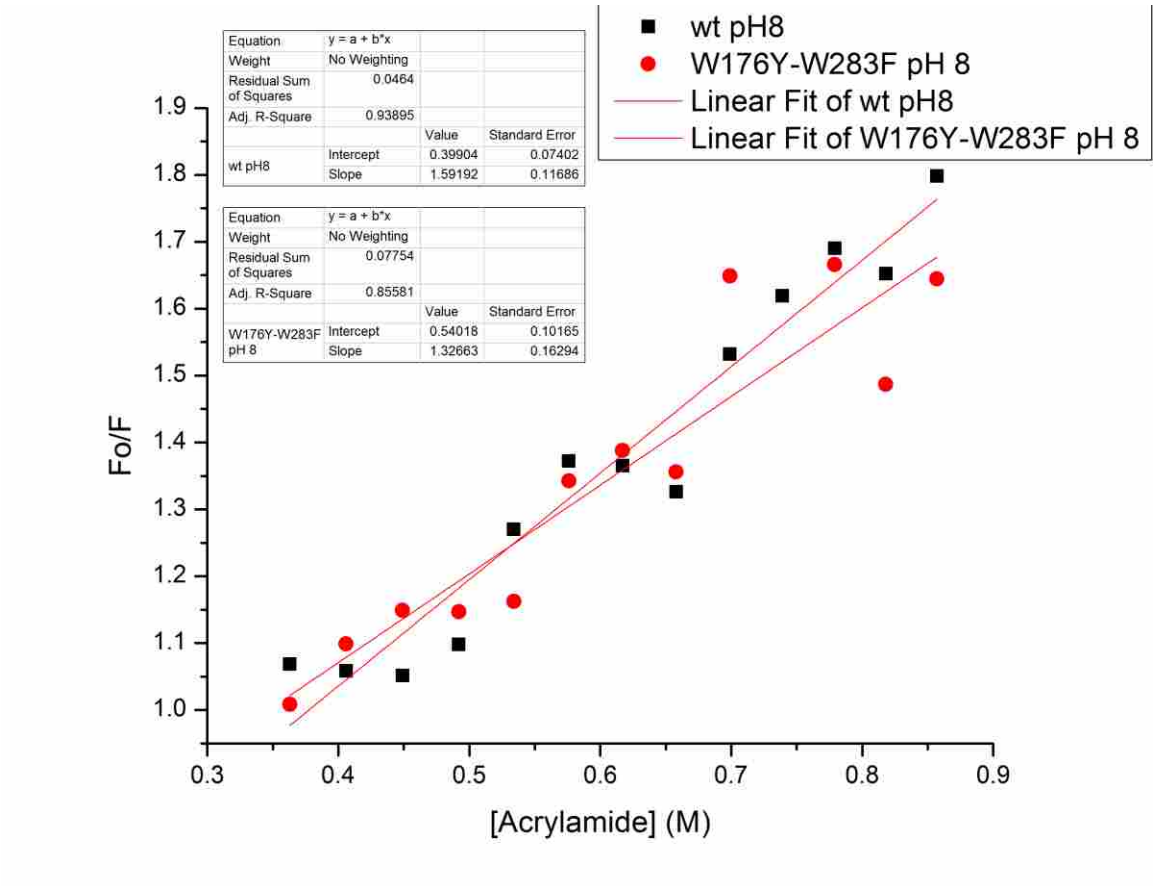

Figure 26: Acrylamide Quenching Data: Stern-Volmer Plot for Quenching of wt UCP2 and W176Y-W283F UCP2 at pH8: Stern-Volmer plot for the results of acrylamide quenching of wt UCP2 and W176Y-W283F UCP2 at pH 8.0 and excitation at 295nm.

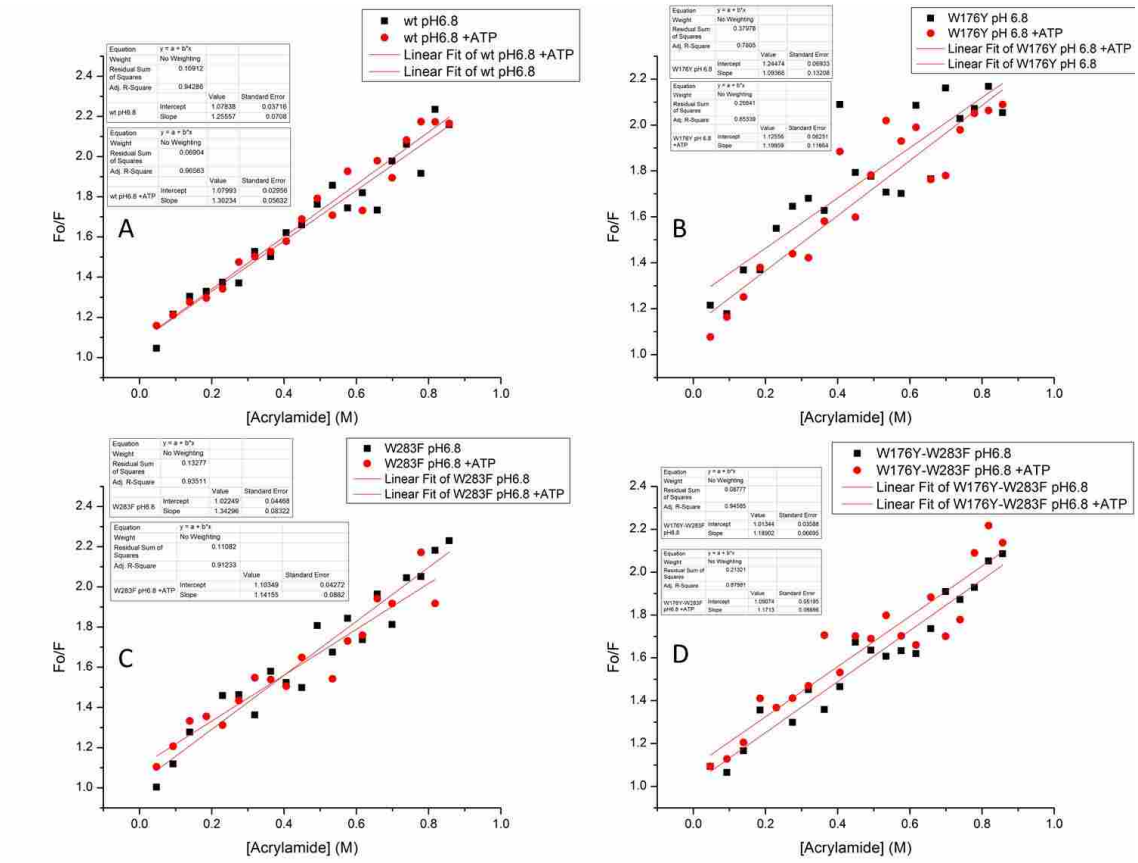

Figure 27: Acrylamide Quenching Data: Stern-Volmer plot for the results of acrylamide quenching of wt (A), W176Y (B), W283F (C) and W176Y-W283F (D) UCP2 at pH 6.8, with and without 100μM ATP and excitation at 295nm.

Table 6: Quenching Constants obtained from Fluorescence Quenching of Selective Trp Mutants of UCP2: Summary of the dynamic quenching constants found for acrylamide quenching of wt and selective Trp mutants of UCP2 with their corresponding standard errors.

UCP2 Mutant	K_d at pH8 (M^{-1})	Std. Error (+/-) (M^{-1})	K_d at pH6.8 No ATP (M^{-1})	Std. Error (+/-) (M^{-1})	K_d at pH6.8 + ATP (M^{-1})	Std. Error (+/-) (M^{-1})
Wt	**1.5919**	0.1169	**1.2556**	0.0708	**1.3023**	0.0563
W176Y	**1.7452**	0.1637	**1.0937**	0.1321	**1.1996**	0.1166
W283F	**2.1408**	0.2894	**1.3430**	0.0832	**1.1416**	0.0882
W176Y-W283F	**1.3266**	0.1629	**1.1890**	0.0670	**1.1713**	0.09896

The fluorescence quenching assays for the UCP2 Trp mutants at pH 8 showed that there was a small increase in the accessibility of the single Trp mutants (W176Y and W283F) to the acrylamide quencher relative to the double mutant but no discernible difference for the single Trp mutants relative to each other (figure 26 and table 6). The results also showed that quenching occurred for wt UCP2 and all of the UCP2 mutants, including the double mutant, which was expected to be completely insensitive to acrylamide quenching (figures 26 and 27D, table 6). Figures 27 and table 6 show the results of the acrylamide quenching experiments at pH6.8, with and without the addition of 100μM ATP. At 100μM ATP UCP2 should be totally inhibited, however the findings show that no significant changes occur in the accessibility of the acrylamide quencher to the Trp residues found in the UCP2

samples upon ATP binding [28]. Furthermore, the results also show that at pH6.8 there is a slight difference in the accessibility of the Trp residues found in the W176Y and W283F samples, with K_d values $1.0937M^{-1}$ +/- $0.1321M^{-1}$ and $1.3430M^{-1}$ +/- $0.0832M^{-1}$, respectively. The results also show a slight difference in the accessibility of Trp residues in the ATP bound wt UCP2 and ATP bound W283F UCP2 samples, with K_d values of $1.3023M^{-1}$ +/- $0.0563M^{-1}$ and $1.1416M^{-1}$ +/- $0.0882M^{-1}$, respectively. The K_d values shown in table 5 also demonstrate a significant decrease in the accessibility of the Trp residues to acrylamide when the pH was lowered from 8 to 6.8.

4.6 Proton Transport Assays for Selective Trp Mutants of UCP2

The final goal of this project was to examine the role of the two Trp residues present in UCP2 in the proton transport activity of the protein. To accomplish this, the proton transport assay that was previously described in [28] was applied to reconstituted samples of wt UCP2 and double mutant UCP2. The results of these assays are shown in figures 28-31 and table 7 shows the computed average specific proton transport rates for each protein. As can been seen in figures 30 and 31 below the W176Y-W283F UCP2 mutant retained proton transport activity but, as shown in table 7, had a decreased specific transport rate relative to the wt protein (2.973101 +/- 0.335897 $\mu mol \cdot min^{-1} \cdot mg\ of\ protein^{-1}$ versus 4.052575 +/- 0.435703$\mu mol \cdot min^{-1} \cdot mg\ of\ protein^{-1}$, respectively).

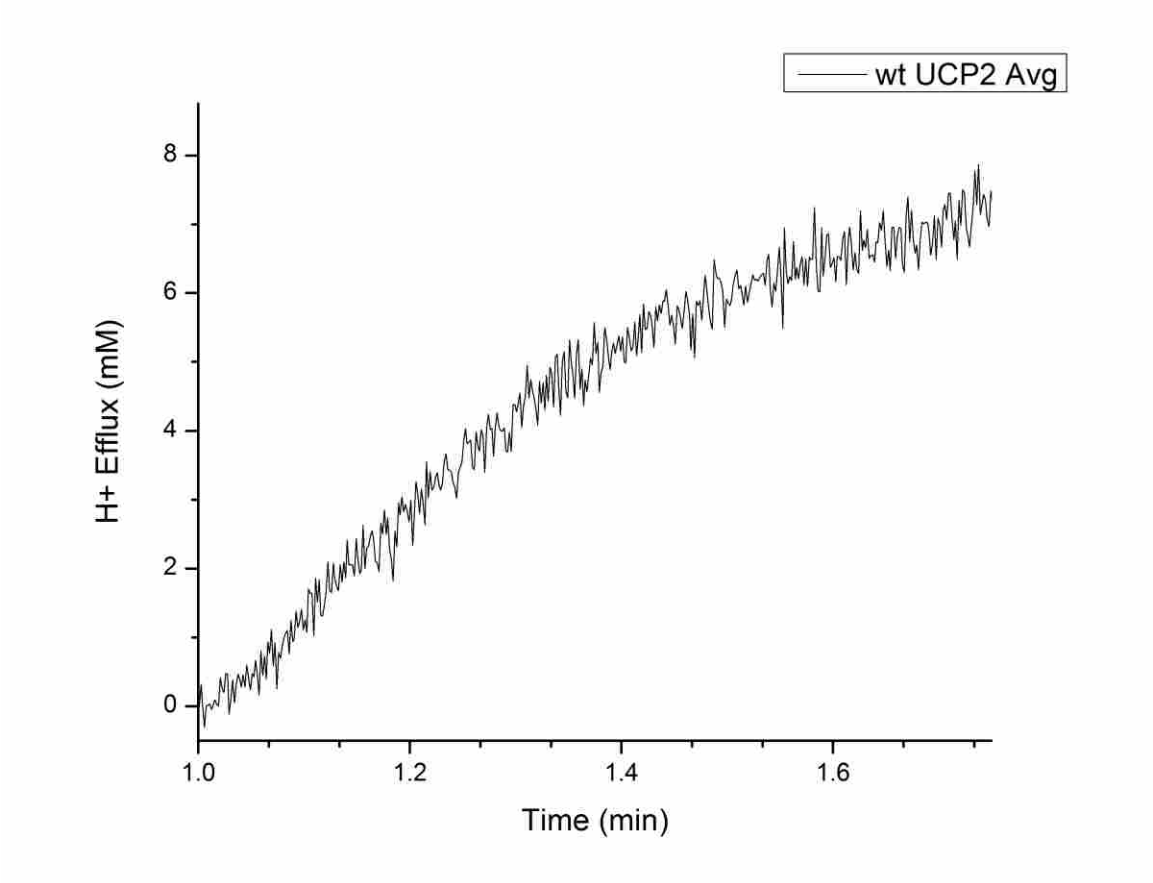

Figure 28: **Proton Flux Rate over Time for the First Round of Proton Transport Assay Applied to wt UCP2:** Average of 5 scans showing proton efflux over time for round 1 of the proton transport assay performed on wt UCP2 reconstituted in L-α-Lecithin.

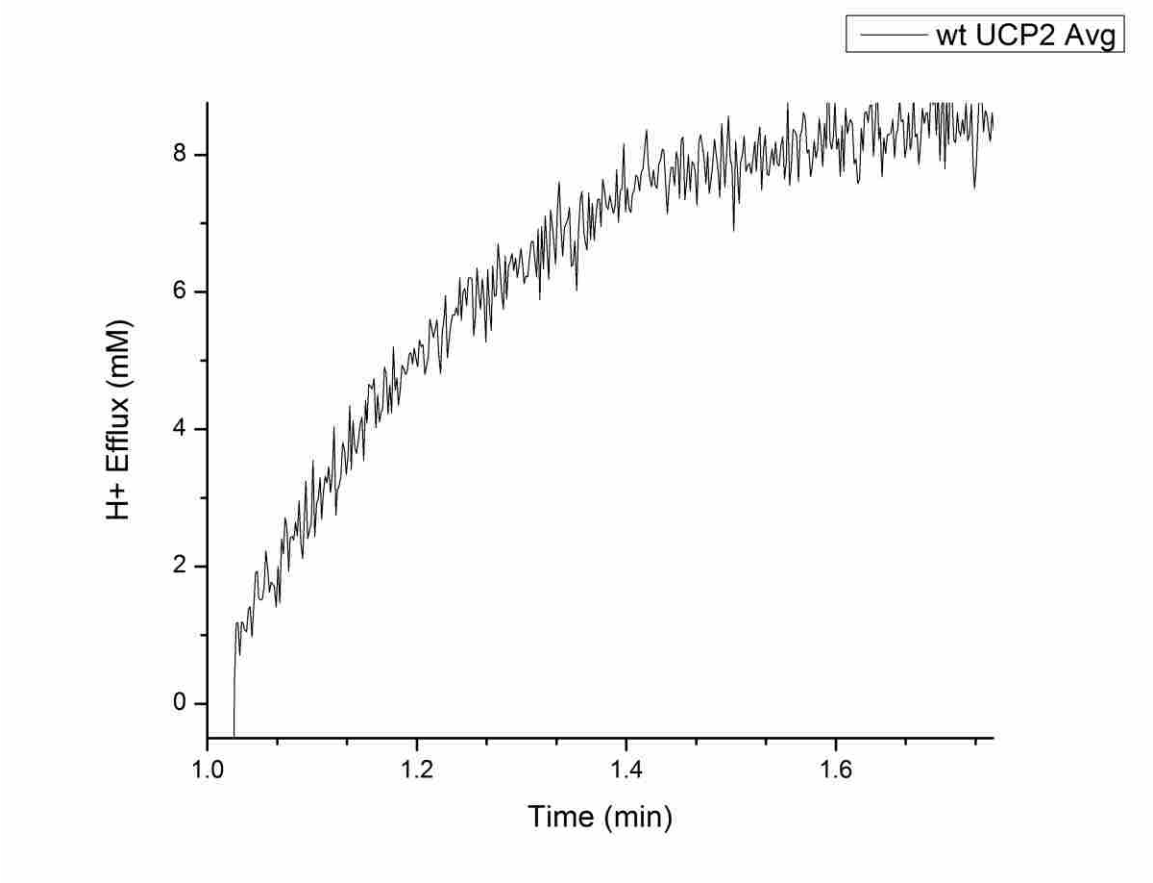

Figure 29: Proton Flux Rate over Time for the Second Round of Proton Transport Assay Applied to W176Y-W283F UCP2: Average of 5 scans showing proton efflux over time for round 2 of the proton transport assay performed on wt UCP2 reconstituted in L-α-Lecithin.

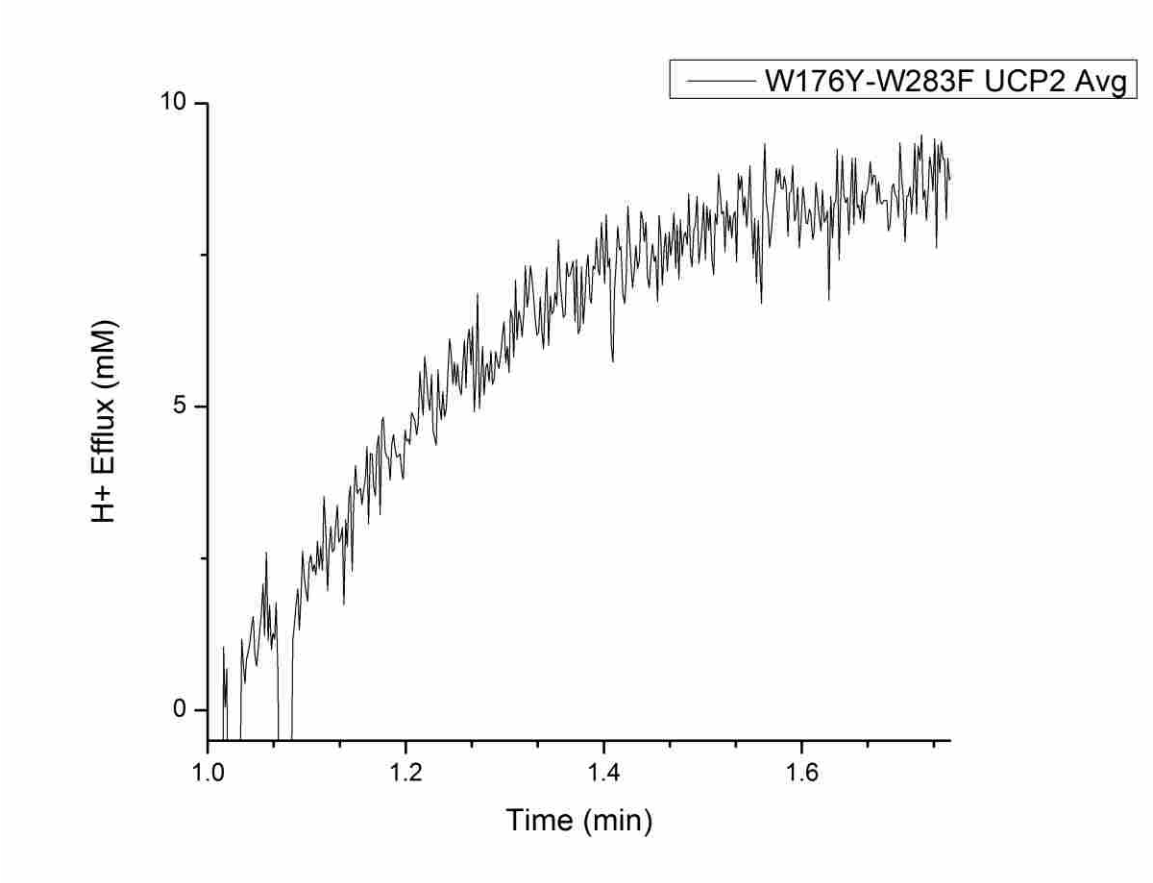

Figure 30: Proton Flux Rate over Time for the First Round of Proton Transport Assay Applied to W176Y-W283F UCP2: Average of 5 scans showing proton efflux over time for round 1 of the proton transport assay performed on W176Y-W283F UCP2 reconstituted in L-α-Lecithin.

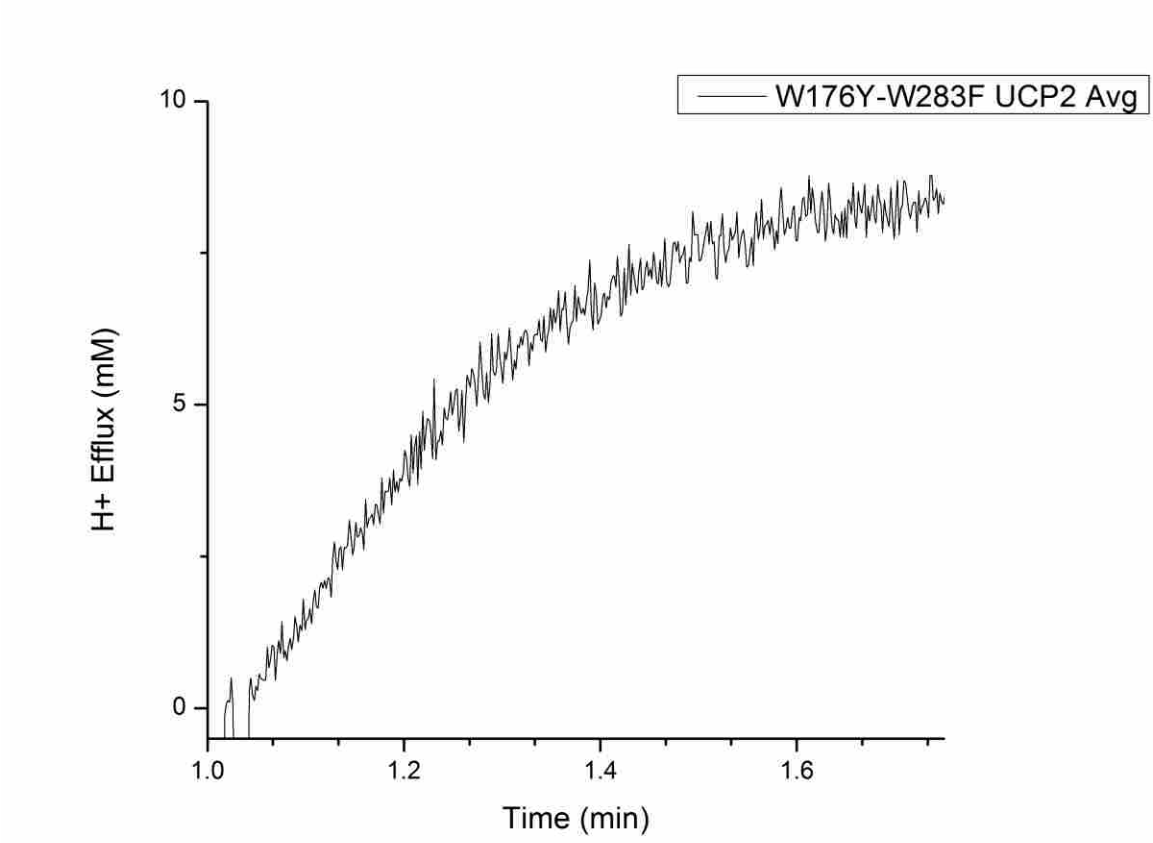

Figure 31: Proton Flux Rate over Time for the Second Round of Proton Transport Assay Applied to W176Y-W283F UCP2: Average of 5 scans showing proton efflux over time for round 2 of the proton transport assay performed on W176Y-W283F UCP2 reconstituted in L-α-Lecithin.

Table 7: Specific Proton Transport Rates for wt and W176-W283F UCP2: Calculated average specific proton transport rates based on the results of two rounds of the proton assay for both wt UCP2 and W176Y-W283F. Reported specific transport rates are the average of 11 scans.

	Wt UCP2	**W176Y-W283F UCP2**
Average Specific Flux Rate ($\mu mol \cdot min^{-1} \cdot mg\ of\ protein^{-1}$)	4.052575	2.973101
Standard error	0.435703	0.335897

5 DISCUSSION

The original objectives of this study, including producing selective Trp mutants of UCP2 cDNA by overlap extension PCR, introducing these mutants into a membrane targeting expression vector, expressing, isolating and purifying UCP2 protein for each of the mutants and the *wt*, confirming that the selective Trp mutants retained conformational equivalence to the *wt* and then running fluorescence spectroscopy based assays on the purified proteins, were successfully completed. However, no clear difference could be observed in the membrane topology of the W176 residue versus the W283 residue, as evidenced by the lack of discernable difference in the accessibility of the two residues to the acrylamide quencher. Another unexpected result was the presence of a fluorescence signal in all double mutant fluorescence scans with excitation at 295nm, which was of a similar magnitude to the fluorescence signal obtained for the Trp containing UCP2 samples. Finally, it was observed that the Trp residues did indeed have an effect on the proton transport activity of UCP2 as evidenced by the marked decrease in the specific transport rate of the W176Y-W283F mutant relative to *wt* UCP2.

5.1 Interpretation of Fluorescence Results

The results of the fluorescence assays performed on UCP2 in detergent appear to show that the W283 residue in UPC2 is normally quenched within the folded protein, as evidenced by the fact that when excited at 295nm the fluorescence spectrum for the W176Y mutant roughly overlaps with that of the

W176Y-W283F double mutant. This conclusion is also supported by the fact that the fluorescence of the W283F mutant roughly overlaps with that of wt UCP2 as the differences between the fluorescence peak of each single Trp mutant with the W176Y-W283F double mutant should be additive to the fluorescence of the wt protein. The results of the SDS denaturation assay (figures 22-23) however, do not support this conclusion as, if this were the case, it would be expected that upon the addition of a denaturant such as SDS the fluorescence signal of the W176Y mutant, when excited at 295nm, would have increased as would that of the wt UCP2, neither of which were observed.

The results of the SDS denaturation assay for W176Y (figure 23B) initially appear to show that ATP does indeed bind in the vicinity of the W283 residue, as expected. This is based on the significantly lower fluorescence signal observed for excitation of W176Y at 295nm upon the addition of 50μM ATP, relative to the W176Y with no ATP added and further supported by the fact that this was no totally mitigated by denaturation with SDS. However, the results of the acrylamide quenching studies (figure 27B and table 6) failed to show any difference in accessibility of the W283 residue to acrylamide quencher in the presence versus absence of 100μM ATP. Taken together these results seem to suggest that the binding of ATP by UCP2 results in a shift in the conformation, as previously shown by CD spectroscopy, leading to increased stability of the local environment around W283 but this should not result in both the blue shift in the peak emission and decrease in fluorescence seen in figure 23B [28]. A similar trend was also obtained for the SDS denaturation assay when it was performed on W283F (figure 23C) but

with the overall decrease in fluorescence upon binding of ATP lessened and an increase in fluorescence observed upon addition of both ATP and SDS, suggesting that binding of ATP destabilizes the environment around W176. The results of the acrylamide quenching assays performed on UCP2 reconstituted into liposomes of L-α-lecithin could not distinguish between the accessibility of the two TRP residues present in UCP2, to the acrylamide quencher and showed no change in the accessibility when 100μM ATP was added, under which conditions UCP2 should be fully inhibited. This contrasts with the work of Viguera *et al.* (1992) which found a significant difference in acrylamide quenching of the two equivalent Trp residues found in UCP1 [60] Unfortunately, the high fluorescence signal, when excited at 295nm, seen for the W176Y-W283F double mutant in all of the fluorescence assays performed, make it impossible to draw any definitive conclusion about the structure or folding of UCP2 in membranes because the fluorescence spectra obtained, as well as any changes within them under differing conditions cannot be related solely to the contributions of the Trp residues found in UCP2.

5.2 Reasons for Tryptophan Fluorescence Signal in Purified W176Y-W283F UCP2

In general, there are only two possible reasons why there could be a fluorescence signal for W176Y-W283F UCP2, when excited at 295nm, given that the DNA sequencing results show correct incorporation of the desired mutations into the UCP2 gene., Either there is significant contamination of the purified UCP2 proteins with another Trp containing protein and thus another source of tryptophan; or there is another fluorophore present in the purified samples with a

similar excitation and emission range to tryptophan. The former, and seemingly more likely, scenario is supported by the observation that the dynamic quenching constants obtained for acrylamide quenching of W176Y-W283F are similar to those obtained for the wt and single Trp mutants of UCP2, as acrylamide should be a specific quencher of Trp fluorescence only [41,61]. However, the presence of bands corresponding to the expected apparent M_w of ~30kDa for UCP2 on anti-his and anti-UCP1 (figures 17 and 18) western blots would seem to suggest that this is not the case. However, the SDS-PAGE gel in figure 19 shows the majority of the protein in the sample is concentrated in a band at 25kDa, which is lower than the expected M_w for UCP2 and therefore may be represent an artifact of the protein expression system, such as a partially expressed truncated UCP2 or significant contamination If this were the case, based on the aforementioned, SDS-PAGE results, the contribution to the spectra of the purified UCP2 samples by non-UCP2 contaminants would be significant and fluorescence scans of the W176Y-W28F mutant excited at 295nm would retain the majority of the fluorescence signal of wt UCP2, as was seen. Therefore, three plausible scenarios remain in which contamination could explain the data obtained. The first is that the band at ~150kDa seen in the SDS-PAGE gel consists of a protein that was co-isolated with UCP2 and which contains significantly more than two Trp residues, all of which are fully solvent exposed, thereby still explaining the lack of signal change in W176Y-W283F after denaturation with SDS. The second is based on the fact that highly hydrophobic membrane proteins may still aggregate under the detergent conditions used for the purification of UCP2 and if the aggregation was strong enough, would not be soluble in SDS and therefore not

seen on an SDS-PAGE gel [62, 63]. The third and final scenario in which contamination with a protein other than UCP2 could explain the resultsis the possibility that UCP2 associates with another protein in the bacterial membrane and in 1% LDAO and 1% OG resulting in the co-purification of the unknown second protein which also has an apparent M_w of ~25kDa on an SDS-PAGE gels. The aforementioned association is then disrupted by the harsher denaturing conditions of SDS-PAGE leading to the purified UCP2 stocks to appear pure but the majority of the protein present is actually UCP2. This scenario may also explain the apparent faintness of the bands seen on the Western blots at ~25kDa relative to the thick dark band seen on the SDS-PAGE gel. To test this possibility a blue native PAGE gel should be run, as this method does not use harsh denaturing conditions like those typically used for SDS-PAGE gels. If this were indeed the case it would be expected that on the blue native PAGE gel the large band at just above the 25kDa mark. Alternatively, to determine if contamination with a non-UCP2 protein is responsible for the band seen at ~25kDa, the band could be excised and subjected to mass spectrometry.

Another seemingly less likely scenario, in which the fluorescence signal seen in W176Y-W283F when excited at 295nm is due to a fluorophore other than tryptophan, but with very tryptophan-like spectral properties, being present in the purified UCP2 samples must be due to some fluorophore present in the samples themselves as it is not observed in blank scans of just the buffer. Given this fact, the only plausible, however still unlikely explanation is that one or more of the 11 tyrosine residues present in wt UCP2 is deprotonated in the ground state under the

scan conditions giving tyrosinate[64-67]. Tyrosinate has a similar emission wavelength to tryptophan, at ~345nm and its fluorescence is virtually indistinguishable from tryptophan and despite the normal pKa value of 10.01 for the phenol group of tyrosine it has previously been reported in proteins at neutral pH [41, 64]. However, in order for this to occur there usually must be an excited state deprotonation of the tyrosine residue by a nearby carboxylic group on an aspartate or glutamate residue. Therefore, since the tyrosine residues should not be appreciably excited at 295nm, especially in the later assays where the excitation slit width was reduced to 2.5nm in order to better control for the possibility of tyrosine emission this is not likely to be the case for UCP2 [64]. Moreover, the fact that the W176Y-W283F mutant was still quenched by acrylamide strongly suggests that tyrosinate fluorescence is not responsible for the unexpected fluorescence results obtained for the double Trp mutant of UCP2.

5.3 The Role of Trp Residues in Proton Transport by UCPs

Tryptophan residues are the largest, most energetically expensive to produce and consequently, the rarest of the 20 standard proteogenic amino acids. Therefore, the presence of two Trp residues that are conserved in all five human uncoupling proteins strongly suggests that they play a critical role in either maintaining the correct folding or in the ion transport activity of the protein. The results of the proton transport assays shown in figures 28-31 and table 7, which show a ~25% decrease in the specific transport rates of W176Y-W283F UCP2 (2.973101 +/- 0.335897 μmol·min^{-1}·mg of protein^{-1} versus 4.052575 +/- 0.435703μmol·min^{-1}·mg of protein^{-1}, respectively) taken together with the established conformational

equivalence of the selective-Trp mutants of UCP2 based on far-UV CD spectroscopy, indicates that the role of the conserved Trp is primarily in the ion transport activity of the UCPs and not in maintaining correct folding of the protein in the membrane. Due to time constraints the proton transport assay was not applied to the single Trp mutants of UCP2 which may have elucidated the relative importance of one Trp residue (W176 or W283) versus the other in the mechanism of proton transport by UCPs.

6 CONCLUSIONS AND FUTURE DIRECTIONS

Three selective Trp mutants of UCP2 have been produced, cloned into the membrane-targeting expression vector pET26b(+) and then transformed into *E.coli* BL21 CD^{+} cells. The results of fluorescence spectroscopy based assay on the selective Trp mutants showed an unexpectedly high fluorescence signal when excited at 295nm that was insensitive to SDS denaturation but quenched by acrylamide, which is normally a specific quencher of Trp fluorescence in proteins. These results suggest significant contamination with one or more other proteins persists after isolation by differential centrifugation and purification by IMAC. The possible reasons leading to this contamination were discussed in section 5.2. In order to definitively establish the presence or absence of Trp in the W176Y-W283F samples the next goal of this project would be to perform Trp amino acid analysis on the purified stocks of each of the selective Trp mutants of UCP2 using the procedure outlined in [61]. If Trp is not detected in the W176Y-W283F samples then this would suggest that the fluorescence observed is either due to another fluorophore present in UCP2 such as a tyrosinate residue or some specific interaction of side chains that occurs in UCP2. Finally, it was observed that the W176Y-W283F UCP2 mutant had an almost 25% decrease in specific proton transport rate relative to the wt protein, suggesting that the two conserved Trp residues found in all human UCPs play a role in mediating the proton transport activity of these proteins. In conclusion, the results of this study seem to suggest that the purification system developed for purifying UCP2 from the membrane-targeted bacterial expression

system does not yield UCP2 at a sufficient degree of purity, contrary to the initial assessment. If this is indeed the case, the problem may be mitigated by modifying the imidazole concentrations used in the IMAC buffers, or if this proves insufficient, by replacing the His-tag with a strep-tag and running on a strep-tactin column [70].

REFERENCES

1. Schefller, I.E. (2011) Mitochondria. Chapter 3, John Wiley and Sons, New York.
2. Affourtit, C., and Brand, M.D. (2009) Measuring Mitochondrial Bioenergetics in INS-1E Insulinoma Cells. *Method. Enzymol.* 457, 405-424.
3. Divakaruni, A.S., and Brand, M.D. (2011) The regulation and physiology of mitochondrial protein leak. *Physiology* 26, 192-205.
4. Brand, M.D. (2000) Uncoupling to survive? The role of mitochondrial inefficiency in ageing. *Exp. Gerontol.* 35, 811-820.
5. Jastroch, M., Divakaruni, A.S., Mookerjee, S., Treberg, J.R., and Brand, M.D. (2010) Mitochondrial proton and electron leaks. *Essay Biochem*. 47, 53-67.
6. Brand, M.D., Chien, L-F., Ainscow, E.K., Rolfe, D.F.S., and Porter, R.K. (1994) The causes and functions of mitochondrial proton leak. *BBA-Bioenergetics* 1187, 132-139.
7. Brand, M.D. (2005) The efficiency and plasticity of mitochondrial energy transduction. *Biochem. Soc. T.* 33, 897-904.
8. Klingenberg, M., and Echtay, K.S. (2001) Uncoupling proteins: the issues from a biochemist point of view. *BBA-Bioenergetics* 1504, 128-143.
9. Echtay, K.S. (2007) Mitochondrial Uncoupling Proteins – What is their Physiological Role? *Free Radic. Biol. Med.* 43, 1351-1371.
10. Nicholls, D.G., Bernson, V.S., and Heaton, G.M. (1978) The identification of the component in the inner membrane of brown adipose tissue mitochondria responsible for regulating energy dissipation. *Exper. Suppl.* 32, 89–93.
11. Esteves, T.C., and Brand, M.D. (2005) The reactions catalysed by the mitochondrial uncoupling proteins UCP2 and UCP3. *BBA-Bioenergetics* 1709, 35-44.
12. Ježek, P., and Urbánková, E. (2000) Specific sequence motifs of mitochondrial uncoupling proteins. *IUBMB Life* 49, 63-70.

13. Berardi, M.J., Shih, W.M., Harrison, S.C., and Chou, J.J. (2011) Mitochondrial uncoupling protein 2 structure determined by NMR molecular fragment searching. *Nature* 476, 109-113.
14. Fiery, C., Neverova, M., Collins, S., Raimbault, S., Champigny, O., Levi-Meyrueis, C., Bouillaud, F., Seldin, M.F., Surwit, R.S., Ricquier, D., and Warden, C.H. (1997) Uncoupling protein-2: a novel gene linked to obesity and hyperinsulinemia. *Nature Gen.* 15, 269-272.
15. Vidal-Puig, A., Solanes, G., Grujic, D., Flier, J.S., and Lowell, B.B. (1997) UCP3: An Uncoupling Protein Homologue Expressed Preferentially and Abundantly in Skeletal Muscle and Brown Adipose Tissue. *Biochem. Bioph. Res. Co.* 235, 79-82.
16. Mao, W., Yu, X.X., Zhong, A., Li, W., Brush, J., Sherwood, S.W., Adasm, S.h., and Pan, G. (1999) UCP4, a novel brain-specific mitochondrial protein that reduces membrane potential in mammalian cells. *FEBS Lett.* 443, 326-330.
17. Sanchis, D., Fleury, C., Chomiki, N., Goubern, M., Huang, Q., Neverova, M., Grégoire, F., Easlick, J., Raimbault, S., Lévi-Meyrueis, C., Miroux, B., Collins, S., Seldin, M., Richard, D., Warden, C., Bouillaud, F., and Ricquier, D. (1998) BMCP1, a Novel Mitochondrial Carrier with High Expression in the Central Nervous System of Humans and Rodents, and Respiration Uncoupling Activity in Recombinant Yeast. *J. Biol. Chem.* 273, 34611-34615.
18. Yu, X.X., Mao, W., Zhong, A., Schow, P., Brush, J., Sherwood, S.W., Adams, S.H., and Pan, G. (2000) Characterization of novel UCP5/BMCP1 isoforms and differential regulation of UCP4 and UCP5 expression through dietary or temperature manipulation. *FASEB J.* 14, 1611-1618.
19. Korshunov, S.S., Skulachev, V.P., and Starkov, A.A. (1997) High protonic potential actuates a mechanism of production of reactive oxygen species in mitochondria. *FEBS Lett.* 416, 15-18.
20. Echtay, K.S., Roussel, D., St-Pierre, J., Jekabson, M.B., Cadensa, S., Stuart, J.A., Harper, J.A., Roebuck, S.J., Morrison, A., Pickering, S., Clapham, J.C., and Brand,

M.D. (2002) Superoxide activates mitochondrial uncoupling proteins. *Nature* 415, 96-99.

21. Echtay, K.S., and Brand, M.D., (2007) 4-Hydroxy-2-nonenal and uncoupling proteins: an approach for regulation of mitochondrial ROS production. *Redox Rep.* 12, 26-29.
22. Murphy, M.P., Echtay, K.S., Blaikie, F.H., Asin-Cayuela, J., Cochemé, H.M., Green, K., Buckingham, J.A., Taylor, E.R., Hurrell, F., Hughes, G., Miwa, S., Cooper, C.E., Svistunenko, D.A., Smith, R.A.J., and Brand, M.D. (2003) Superoxide activates uncoupling proteins by generating carbon-centered radicals and initiating lipid peroxidation studies using a mitochondria-targeted spin trap derived from α-phenyl-*n*-*tert*-butylnitrone. *J. Biol. Chem.* 278, 48534-48545.
23. Krauss, S., Zhang, C-Y., and Lowell, B.B. (2005) The mitochondrial uncoupling protein homologues. *Nat. Rev. Mol. Cell Bio.* 6, 248-261.
24. Klingenberg, M., and Echtay, K.S. (2001) Uncoupling proteins: the issues from a biochemist point of view. *BBA-Bioenergetics* 1504, 128-143.
25. Echtay, K.S., Winkler, E., Bienengraeber, M., and Klingenberg, M. (2000) Site-directed mutagenesis identifies residues in uncoupling protein (UCP1) involved in three different functions. *Biochemistry* 39, 331-3317.
26. Garlid, K.D., Jabůrek, M., and Ježek, P. (1998) The mechanism of proton transport mediated by mitochondrial uncoupling proteins. *FEBS Lett.* 438, 10-14.
27. Rial, E., Aguirregoitia, E., Jesús, J-J., and Ledesma, A. (2004) Alkylsulfonates activate the uncoupling protein UCP1: implications for the transport mechanism. *BBA-Bioenergetics* 1608, 122-130.
28. Hoang, T, Smith, M.D., and Jelokhani-Niaraki, M. (2012) Toward understanding the mechanism of ion transport activity of neuronal uncoupling Proteins UCP2, UCP4, and UCP5. *Biochemistry* 51, 4004-4014.
29. Robinson, A.J., Overy, C., and Kunji E.R.S. (2008) The mechanism of transport by mitochondrial carriers based on analysis of symmetry. *Proc. Natl. Acad. Sci. USA* 105, 17766-17771.

30. Yu, X., Wieczorek, S., Franke, A., Yin, H., Pierer, M., Sina, C., Karlsen, T.H., Boberg, K.M., Bergquist, A., Kunz, M., Witte, T., Gross, W.L., Epplen J.T., Alarcón-Riquelme, M.E., Schreiber, S., and Ibrahim, S.M. (2009) Association of UCP2 −866 G/A polymorphism with chronic inflammatory diseases. *Genes Immun.* 10, 601-605.
31. Esterbauer, H., Schneitler, C., Oberkofier, H., Ebenbichier, C., Paulweber, B., Sandhofer, F., Ladurner, G., Hell, E., Strosberg, D., Patsch, J.R., Krempler, F., and Patsch, W. (2001) A common polymorphism in the promoter of *UCP2* is associated with decreased risk of obesity in middle-aged humans. *Nat. Genet.* 28, 178-183.
32. Snyder, E.E., Walts, B., Pérusse, L., Chagnon, Y.C., Weisnagel, S.J., Rankinen, T., and Bouchard, C. (2012) The Human Obesity Gene Map: The 2003 Update. *Obes. Res.* 12, 369,439.
33. Ježek, P., Olejár, T., Smolková, K., Ježek, J., Dlasková, A., Plecitá-Hlavatá, L., Zelenka, J., Špaček, T., Engstová, H., Pajuelo-Reguera, D., Jabůrek, M. (2014) Antioxidant and regulatory role of mitochondrial uncoupling protein UCP2 in pancreatic β-cells. *Physiol. Res*. 63 (2014) 73-91.
34. Robson-Doucette, C.A., Sultan, S., Allister, E.M., Wikstrom, J.D., Koshkin, V., Bhattacharjee, A., Prentice, K.J., Sereda, S.B., Shirihai, O.S., and Wheeler, M.B. (2011) β-Cell uncoupling protein 2 regulates reactive oxygen species production, which influences both insulin and glucagon secretion. *Diabetes* 60, 2710-2719.
35. Krauss, S., Zhang, C.-Y., Scorrano, L., Dalgaard, L.T., St-Pierre, J., Grey, S.T., and Lowell, B.B. (2003) Superoxide-mediated activation of uncoupling protein 2 causes pancreatic β-cell dysfunction. *J. Clin. Invest*. 112, 1831-1842.
36. Affourtit, C., and Brand, M.D. (2008) On the role of uncoupling protein-2 in pancreatic beta cells. *Biochim. Biophys. Acta* 1777, 973-979.
37. Pecqueur, C., Alves,Guerra, M.-C., Gelly, C., Lévi-Meyrueis, C., Couplan, E., Collins, S., Ricquier, D., Bouillaud, F., and Miroux, B. (2001) Uncoupling Protein

2, *in vivo* distribution, induction upon oxidative stress, and evidence for translational regulation. *J. Biol. Chem*. 276, 8705-8712.

38. Donadelli, M., Dando, I, Fiorini, C., and Palmieri, M. (2014) UCP2, a mitochondrial protein regulated at multiple levels. *Cell. Mol. Life Sci.* 71, 1171-1190.

39. PDB ID: 2LCK. Berardi, M.J., Shih, W.M., Harrison, S.C., Chou, J.J...

40. Ivanova, M.V., Hoang, T., McSorley, F.R., Krnac, G., Smith, M.D., and Jelokhani-Niaraki, M. (2010) A comparative study on conformation and ligand binding of the neuronal uncoupling protein. *Biochemistry* 49, 512-521.

41. Lakowicz, J.R. (2007) Principles of Fluorescence Spectroscopy. Springer, New York.

42. Eftink, M.R. (2002) Fluorescence Quenching: Theory and Application. *Topics in Fluorescence Spectroscopy* 2, 53-126.

43. Aiyar, A., Xiang, Y., Leis, J. (1996) Site-directed mutagenesis by overlap extension using polymerase chain reaction. *Methods in Molecular Biology*. 57:177-191.

44. Heckman K.L., Pease L.R., Gene splicing and mutagenesis by PCR-driven overlap extension. (2007) *Nat. Protoc.* 2(4) 924-932.

45. Kelly, S.M., Jess, T.J., and Price, N.C. How to study proteins by circular dichroism. (2005) *BBA–Proteins Proteom* 1751, 119-139.

46. Greenfield, N.J. Methods to Estimate the Conformation of Proteins and Polypeptides from Circular Dichroism Data. (1996) *Anal Biochem* 235, 1-10.

47. Ladokhin, A.S., Jayasinghe, S., White, S.H. How to Measure and Analyze Tryptophan Fluorescence in Membranes Properly, and Why Bother? (2000) *Anal Biochem* 285(2), 235-245.

48. Moro, F., Felix, M., Goni, M., Angeles, U. (1993) Fluorescence quenching at interfaces and the permeation of acrylamide and iodide across phospholipid bilayers. *Biochemistry*. 330(2), 129-132.

49. Promega Corporation: Wizard® Plus SV Minipreps DNA Purification System Technical Bulletin. Accessed 9/06/2015.

50. Promega Corporation: Wizard® SV Gel and PCR Clean-Up System Technical Bulletin Accessed 9/06/2015.

51. Qiagen: HotStar HiFidelity PCR Handbook. Accessed 09/06/2015

52. Studier, F.W. (2005) Protein production by auto-induction in high-density shaking cultures. *Protein Expres. Purif.* 41, 207-234.

53. Qiagen: The QIAexpressionist. Accessed 11/06/2015.

54. Bio-Rad: Instruction Manual, Bio-Rad Protein Assay. Accessed 11/06/2015.

55. Bio-Rad: Econo-Pac® 10DG Columns Instruction Manual. Accessed 11/06/2015.

56. Hoang, T. Conformation and ion transport of neuronal uncoupling proteins: UCP2, UCP4, and UCP5. (2011) M.Sc. Thesis. Wilfrid Laurier University.

57. Hoang, T., Smith, M.D., and Jelokhani-Niarako, M. (2013) Expression, folding, and proton transport activity of human uncoupling protein-1 (UCP1) in lipid membranes: evidence for associated functional forms. *J. Biol. Chem.* 288, 36244-3624458.

58. Madden, T. Chapter 16: The BLAST Sequence Analysis Tool. *The NCBI Handbook.*(2002). U.S. National Library of Medicine (Bethesda, MD, USA).

59. Hoang, T., Matovic, T., Parker J, Smith, M.D., Jelokhani-Niaraki, M. Role of positively charged residues of the second transmembrane domain in the ion transport activity and conformation of human uncoupling protein-2. (2015) *Biochemistry.* 54(14), 2303-2313.

60. Viguera, A.R., Goñi, F.M., and Rial, E. (1992) The uncoupling protein from brown adipose tissue mitochondria: The environment of the tryptophan residues as revealed by quenching of intrinsic fluorescence. *Eur. J. Biochem.* 210, 893-899.

61. Hof, Martin, Rudolf Hutterer, and Vlastimil Fidler. Fluorescence spectroscopy in biology: advanced methods and their applications to membranes, proteins, DNA, and cells. (2005) Vol. 3. Springer Science & Business Media. (Berlin, Germany).

62. Anatrace. Detergents and Their Uses in Membrane Protein Science. Accessed 14/06/2015.
63. Sagné, C., Isambert, M.F., Henry, J.P., Gasnier, B. SDS-resistant aggregation of membrane proteins: application to the purification of the vesicular monoamine transporter. (1996) 316(3) 825-831.
64. Szabo, A.G., Lynn, K., Krajcarski, D., Rayner D.M. Tyrosine fluorescence at 345 nm in proteins lacking tryptophan. (1979) *JOL* 18-19, 582-586.
65. Permyakov, Eugene A. Luminescent spectroscopy of proteins. (1992.) CRC press (Boca Raton, FL, USA).
66. Pundak S., Roche, R.S., Tyrosine and tyrosinate fluorescence of bovine testes calmodulin: calcium and pH dependence. (1984) *Biochemistry* 23(7) 1549-1555.
67. Prendergast, F. G., Hampton, P. D., & Jones, B. Characteristics of tyrosinate fluorescence emission in. alpha.-and. beta.-purothionins. Biochemistry, (1984) 23(26), 6690-6697.
68. Oelshlegel, F. J., Jr., Schroeder, J. R., Stahmann, M. A. A simple procedure for basic hydrolysis of proteins and rapid determination of tryptophan using a starch column. (1970) *Anal. Biochem.* 34, 331
69. Sprenger, G.A., Aromatic Amino Acids in *Amino Acid Biosynthesis – Pathways, Regulation and Metabolic Engineering* (Wendisch, V.F.) (2007) 94-116. Springer Science & Business Media. (Berlin, Germany).
70. Schmidt, T.G.M., Skerra, A., The Strep-tag system for one-step purification and high-affinity detection or capturing of proteins. (2007) *Nat. Protoc.* 2, 1528-1535.

M.Sc. Thesis Appendix

Appendix 1: Full Primer List for PCR

	Forward Primer	Reverse Primer
UCP2 Flanking Primers	5'GGAGATATACCCATGGGAGGATCGCATCACC'3	5'CGCAAGCTTGTCGACGGAGCTCTTAGAAGGG'3
NcoI Removal Primers	5'-GCACCATTCTGACTATGGTGCGTACTGAGG-3'	5'-CCTCAGTACGCACCATAGTCAGAATGGTGC-3'
W176Y Primers	5'GGGTTCCGGGGCCTCTACAAAGGGACCTCTCCC'3	5'GGGAGAGGTCCCTTTGTAGAGGCCCCGGAACCC'3
W283F Primers	5' CTCCGCTTGGGTTCCTTCAACGTGGTGATGTTC 3'	5'GAACATCACCACGTTGAAGGAACCCAAGCGGAG'3

Appendix 2: Sequencing Results

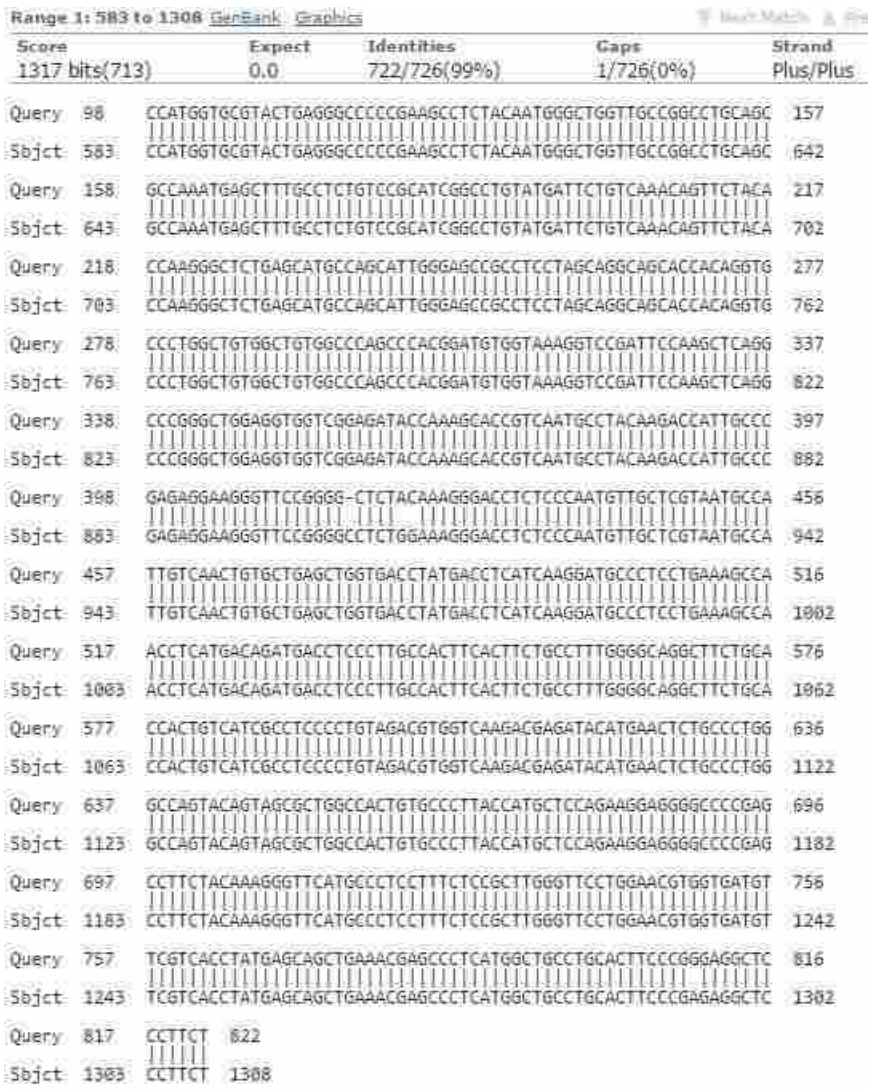

Range 1: 583 to 1308 GenBank Graphics

Score	Expect	Identities	Gaps	Strand
1317 bits(713)	0.0	722/726(99%)	1/726(0%)	Plus/Plus

```
Query  98    CCATGGTGCGTACTGAGGGCCCCCGAAGCCTCTACAATGGGCTGGTTGCCGGCCTGCAGC  157
             ||||||||||||||||||||||||||||||||||||||||||||||||||||||||||||
Sbjct  583   CCATGGTGCGTACTGAGGGCCCCCGAAGCCTCTACAATGGGCTGGTTGCCGGCCTGCAGC  642

Query  158   GCCAAATGAGCTTTGCCTCTGTCCGCATCGGCCTGTATGATTCTGTCAAACAGTTCTACA  217
             ||||||||||||||||||||||||||||||||||||||||||||||||||||||||||||
Sbjct  643   GCCAAATGAGCTTTGCCTCTGTCCGCATCGGCCTGTATGATTCTGTCAAACAGTTCTACA  702

Query  218   CCAAGGCTCTGAGCATGCCAGCATTGGGAGCCGCCTCCTAGCAGGCAGCACCACAGGTG  277
             ||||||||||||||||||||||||||||||||||||||||||||||||||||||||||||
Sbjct  703   CCAAGGCTCTGAGCATGCCAGCATTGGGAGCCGCCTCCTAGCAGGCAGCACCACAGGTG  762

Query  278   CCCTGGCTGTGGCTGTGGCCCAGCCCACGGATGTGGTAAAGGTCCGATTCCAAGCTCAGG  337
             ||||||||||||||||||||||||||||||||||||||||||||||||||||||||||||
Sbjct  763   CCCTGGCTGTGGCTGTGGCCCAGCCCACGGATGTGGTAAAGGTCCGATTCCAAGCTCAGG  822

Query  338   CCCGGGCTGGAGGTGGTCGGAGATACCAAAGCACCGTCAATGCCTACAAGACCATTGCCC  397
             ||||||||||||||||||||||||||||||||||||||||||||||||||||||||||||
Sbjct  823   CCCGGGCTGGAGGTGGTCGGAGATACCAAAGCACCGTCAATGCCTACAAGACCATTGCCC  882

Query  398   GAGAGGAAGGGTTCCGGGG-CTCTACAAAGGGACCTCTCCCAATGTTGCTCGTAATGCCA  456
             |||||||||||||||||| ||||  ||||||||||||||||||||||||||||||||||||
Sbjct  883   GAGAGGAAGGGTTCCGGGGCCTCTGGAAAGGGACCTCTCCCAATGTTGCTCGTAATGCCA  942

Query  457   TTGTCAACTGTGCTGAGCTGGTGACCTATGACCTCATCAAGGATGCCCTCCTGAAAGCCA  516
             ||||||||||||||||||||||||||||||||||||||||||||||||||||||||||||
Sbjct  943   TTGTCAACTGTGCTGAGCTGGTGACCTATGACCTCATCAAGGATGCCCTCCTGAAAGCCA  1002

Query  517   ACCTCATGACAGATGACCTCCCTTGCCACTTCACTTCTGCCTTTGGGGCAGGCTTCTGCA  576
             ||||||||||||||||||||||||||||||||||||||||||||||||||||||||||||
Sbjct  1003  ACCTCATGACAGATGACCTCCCTTGCCACTTCACTTCTGCCTTTGGGGCAGGCTTCTGCA  1062

Query  577   CCACTGTCATCGCCTCCCCTGTAGACGTGGTCAAGACGAGATACATGAACTCTGCCCTGG  636
             ||||||||||||||||||||||||||||||||||||||||||||||||||||||||||||
Sbjct  1063  CCACTGTCATCGCCTCCCCTGTAGACGTGGTCAAGACGAGATACATGAACTCTGCCCTGG  1122

Query  637   GCCAGTACAGTAGCGCTGGCCACTGTGCCCTTACCATGCTCCAGAAGGAGGGGCCCCGAG  696
             ||||||||||||||||||||||||||||||||||||||||||||||||||||||||||||
Sbjct  1123  GCCAGTACAGTAGCGCTGGCCACTGTGCCCTTACCATGCTCCAGAAGGAGGGGCCCCGAG  1182

Query  697   CCTTCTACAAAGGGTTCATGCCCTCCTTTCTCCGCTTGGGTTCCTGGAACGTGGTGATGT  756
             ||||||||||||||||||||||||||||||||||||||||||||||||||||||||||||
Sbjct  1183  CCTTCTACAAAGGGTTCATGCCCTCCTTTCTCCGCTTGGGTTCCTGGAACGTGGTGATGT  1242

Query  757   TCGTCACCTATGAGCAGCTGAAACGAGCCCTCATGGCTGCCTGCACTTCCCGGGAGGCTC  816
             |||||||||||||||||||||||||||||||||||||||||||||||||| |||||||||
Sbjct  1243  TCGTCACCTATGAGCAGCTGAAACGAGCCCTCATGGCTGCCTGCACTTCCCGAGAGGCTC  1302

Query  817   CCTTCT  822
             ||||||
Sbjct  1303  CCTTCT  1308
```

W176Y Forward Sequencing with T7 Primer

W283F Reverse Sequencing with T7 Terminator Primer